Journal of Neural Engineering



# Methods of poly (3,4)-ethylenedioxithiophene (PEDOT) electrodeposition on metal electrodes for neural stimulation and recording

To cite this article before publication: Thomas Niederhoffer *et al* 2023 *J. Neural Eng.* in press https://doi.org/10.1088/1741-2552/acb084

**Review Article**

# Methods of poly(3,4)-ethylenedioxithiophene (PEDOT) electrodeposition on metal electrodes for neural stimulation and recording

**Thomas Niederhoffer [1], Anne Vanhoestenberghe [2], and Henry T. Lancashire [1,†]**

[1] Department of Medical Physics and Biomedical Engineering, University College London, WC1E 6BT, UK

[2] School of Biomedical Engineering and Imaging Sciences, King's College London, UK; a.vanhoest@kcl.ac.uk

E-mail: [†] h.lancashire@ucl.ac.uk

May 2022

**Abstract.** Conductive polymers are of great interest in the field of neural electrodes because of their potential to improve the interfacial properties of electrodes. In particular, the conductive polymer poly (3,4)-ethylenedioxithiophene (PEDOT) has been widely studied for neural applications. This review compares methods for electrodeposition of PEDOT on metal neural electrodes, and analyses the effects of deposition methods on morphology and electrochemical performance. The findings of this review show that: coating thickness and charge storage capacity are positively correlated with PEDOT electrodeposition charge density. We also show that PEDOT coated electrode impedance at 1 kHz, the only consistently reported impedance quantity, is strongly dependent upon electrode radius across a wide range of studies, because PEDOT coatings reduces the reactance of the complex impedance, conferring a more resistive behavior to electrodes (at 1 kHz) dominated by the solution resistance and electrode geometry. This review also summarises how PEDOT co-ion choice affects coating structure and morphology and shows that co-ions notably influence the charge injection limit but have a limited influence on charge storage capacity and impedance. Finally we discuss the possible influence of characterisation methods to assess the robustness of comparisons between published results using different methods of characterisation.

Submitted to: *J. Neural Eng.*

## 1. Introduction

Neural interfaces for nerve recording and stimulation are used from basic neuroscience to clinical diagnosis and therapies. Electrical stimulation and neural recording require high quality interfaces with neural tissue. Neural interfaces comprise one or more electrodes which form the connection between the electron conductors in recording and stimulating electronics, and the ionic conductor of the body tissue across which electrical charge may move (Boehler et al.; 2020). This article reviews coatings on metallic neural electrodes formed by electrodeposition of the conductive polymer poly(3,4)-ethylenedioxythiophene (PEDOT), a popular electrode coating for next generation neural implants.

This review aims to map out PEDOT electrodeposition methods, highlight the relationships between electrodeposition methods and the physical and electrochemical properties of electrodeposited PEDOT neural electrodes. First, an overview of key electrochemical properties of neural electrodes and methods of electrochemical characterisation is given. Second, conducting polymers including PEDOT are introduced and conductive polymer electrode manufacturing methods are discussed. Third, we present the methods for our review, including search strategy, inclusion and exclusion criteria, data extraction, and analysis. Fourth, we analyse the PEDOT electrodeposition materials and methods choices made across the literature. Fifth, we analyse the coating characterisation methods used for electrodeposited PEDOT neural electrodes. Sixth, coating morphology is analysed including coating thickness and roughness. Seventh, the electrochemical performance of electrodeposited PEDOT is analysed with respect to the electrodeposition materials and methods choices. Finally the findings of this review are discussed, additional aspects of PEDOT coating analysis are addressed, and brief conclusions on the use of electrodeposited PEDOT for neural electrodes are drawn.

### *1.1. Neural Electrode Physical and Electrochemical Properties*

Neural electrodes placed in or on the body must perform their required function without causing excessive harm to either body tissues or the electrode or electronics themselves, with the electrode properties tailored to the application. Electrode mechanical properties must also be considered, mismatch between neural tissue and electrode array stiffness and rheology can lead to relative micromotion exacerbating the local foreign body response and degrading long term device performance (Liu et al.; 2020). Electrodes and electrode arrays are becoming increasingly miniaturised to reduce tissue damage during implantation and to increase spatial resolution with multiple electrodes within a small tissue volume. Miniaturisation reduces the electrode geometric surface area (GSA), while the real electrode surface area (RSA) may be greater than the GSA due to electrode roughness and porosity (Cogan; 2008).

Neural electrodes for recording from the nervous system will ideally transmit the neural signal from the body to the recording electronics with minimum distortion and attenuation (Boehler et al.; 2020). In practice the electrochemical properties of real

electrodes act to attenuate, filter, and introduce noise to neural recordings (Guo; 2020; Fan et al.; 2021; Mierzejewski et al.; 2020). Electrochemical properties of an electrode of interest (the working electrode, WE) are measured in a two-electrode or three-electrode electrochemical cell (figure 1B). In a two-electrode cell a counter electrode (CE) acts as both a current source/sink to complete the circuit with the WE, and also as a point against which the WE potential is measured. However, if the passage of current affects the potential of the non-WE a three-electrode cell must be used. In the three-electrode cell current still flows between WE and CE, and the WE potential is measured against a third reference electrode (RE) with a known stable electrode potential, through which negligible current flows (Bard and Faulkner; 2001).

The electrochemical property of electrodes most considered in neural recordings is the complex impedance ($Z_e$), the opposition to alternating current. Electrode impedance is measured with electrochemical impedance spectroscopy (EIS), a small amplitude sinusoidal voltage or current is applied to the electrode over a range of frequencies and the arising current or voltage is measured (figure 1D) (Cogan; 2008). The small amplitude EIS signals aim to achieve a pseudo-linear current:voltage response, and are relevant to recording small amplitude neural signals. Measurements of complex electrode impedance are commonly fitted to equivalent circuits which aim to describe the physical charge transfer mechanisms in terms of discrete circuit elements. A simple equivalent circuit for a single electrode in a solution (or electrolyte) is given in figure 1A.

Complex impedance is commonly reported as magnitude ($|Z_e|$, $\Omega$) and phase angle ($\phi$,$^\circ$) against axes of frequency in a Bode plot (figure 1Diii). Nyquist plots of imaginary part($Z_e''$, $\Im(Z_e)$) against real part($Z_e'$, $\Re(Z_e)$) of the impedance on the complex plane are also used for interpretation, though Nyquist plots lack frequency information (figure 1Dii). The real (resistive, 0° phase) and imaginary (reactive, ±90° phase) parts of the complex impedance must not be mistaken for the respective resistor ($R_f$,$R_s$) and capacitor ($C_{dl}$) components in an equivalent circuit, instead $\Re(Z_e)$ and $\Im(Z_e)$ must be found from the impedance function, which we give for figure 1A in equation 1, where $j$ is the imaginary unit and $\omega$ is angular frequency in $rad \cdot s^{-1}$ ($\omega = 2\pi f$, $f$ in Hz).

$$Z_e = R_s + \frac{R_f}{1 + j\omega C_{dl} R_f} \tag{1}$$

On insertion of an electrode into a solution electric charges redistribute at the interface to form a double layer capacitance ($C_{dl}$). This capacitance comprises the complementary movement of electron and ionic charges in the electrode and solution respectively, the adsorbtion of ions to the electrode surface, and the (re-)orientation of polar molecules including water at the interface (Merrill et al.; 2005; Guo; 2020). For metal neural electrodes $C_{dl}$ typically ranges from 10 $\mu F \cdot cm^{-2}$ to 20 $\mu F \cdot cm^{-2}$ of real electrode surface area (Merrill et al.; 2005). Charge injection through $C_{dl}$ involves no movement of electrons across the interface, and is reversible, however the amount of charge which can be injected capacitively is typically small.

Charge injection involving electron transfer across the interface (Faradaic charge transfer) comprises oxidation and reduction of the electrode and/or solution. The

Faradaic impedance ($R_f$) represents the resistance to these charge transfer processes, and may also include Warburg equivalent circuit elements modelling diffusion of Faradaic reactants to the interface (Mierzejewski et al.; 2020). Faradaic reactions may be irreversible if the products of a forward reaction are no longer present at the interface for the reverse reaction, for example reaction products which diffuse away from the interface, or become unavailable because the products have entered another phase (precipitating as a solid, or being evolved as a gas) (Merrill et al.; 2005). In the case of neural recording, little to no faradaic charge transfer takes place at the interface and mainly capacitive charge redistribution occurs, thus for recording $R_f$ may be considered open circuit (Guo; 2020).

$R_s$ represents the resistance of a solution or body tissue between an electrode and a remote point in the solution. For a planar disc electrode the solution resistance ($R_s$) depends upon the bulk resistivity ($\rho$) and the electrode radius ($r$) according to Newman (1966):

$$R_s = \frac{\rho}{4r} \tag{2}$$

At neural recording relevant frequencies $R_s$ may be considered resistive (Guo; 2020).

The electrode potential ($V_{ee}$) arises due to electron transfer between the electrode and solution reaching equilibrium (Merrill et al.; 2005). $V_{ee}$ depends upon the electrode material, solution, and environmental conditions and may have an amplitude of hundreds of mV at equilibrium with no current flow (Guo; 2020). In practice the electrode potential is not measured in isolation, but must be measured with respect to RE with a known stable electrode potential. The potential measured between WE and RE when no current flows is termed the open circuit potential (OCP), where WE has no redox couple present setting the electrode potential under equilibrium conditions (often the case for neural electrodes), OCP must be experimentally determined (Bard and Faulkner; 2001). Typically EIS is carried out at the OCP to probe the electrode properties near to zero current conditions.

The electrode impedance influences the quality of neural recordings. The real component of the impedance $\Re(Z_e)$ contributes Johnson–Nyquist (thermal) noise to recordings according to:

$$v_{n,rms} = \left(4k_bT \int_{f_1}^{f_2} \Re(Z_e)df\right)^{-\frac{1}{2}} \tag{3}$$

where $v_{n,rms}$ is the root mean squared thermal noise voltage, $k_b$ is Boltzmann's constant ($1.380649 \times 10^{-23} J \cdot K^{-1}$, $T$ is the temperature in $K$, $f_1$ to $f_2$ is the recording bandwidth, and $\Re(Z_e)$ is the real component of the impedance at $f$ (Mierzejewski et al.; 2020; Boehler et al.; 2020). Large electrode impedances may contribute significant noise, for example an electrode with $\Re(Z_e) = 1\ M\Omega$, across a bandwidth of 100 Hz to 10 kHz, at body temperature, has a thermal noise of $v_{n,rms} \approx 13\ \mu V_{rms}$. The electrode impedance also forms a voltage divider with the recording amplifier input impedance $Z_{in}$ according to equation 4, attenuating the signal at the electrode interface $V_S$ to the voltage at

the amplifer input $V_{in}$ and contributes a high-pass filter comprising $C_{dl}$ and the input impedance of the biosignal recording amplifier (Guo; 2020).

$$V_{in} \approx \frac{Z_{in}}{Z_e + Z_{in}} V_S \tag{4}$$

For differential neural recordings, impedance imbalance between electrodes degrades the effective system common mode rejection ratio ($CMRR$) according to 5. Common mode signal ($V_{cm}$) is common to both differential amplifier inputs and includes unwanted artefacts such as DC electrode potential offsets and power line interference. $CMRR$ is the ratio of differential gain ($A_d$) to common mode gain ($A_{cm}$). For electrodes with impedances $Z_{e,1}$ and $Z_{e,2}$ the amplified output voltage is:

$$V_{out} \approx A_d \left( V_S + V_{cm} \frac{Z_{e,2} - Z_{e,1}}{Z_{in}} \pm \frac{V_{cm}}{CMRR} \right) \tag{5}$$

Therefore reducing electrode impedance will improve neural recordings by reducing thermal noise (equation 3), minimising signal attenuation (equation 4), and minimising electrode impedance imbalance ($Z_{e,2} - Z_{e,1}$) (equation 5).

Where electrodes are used for neural stimulation, charge is injected across the electrode solution interface. The aim of stimulation is to change the transmembrane potential of nearby excitable cells, initiating or blocking action potentials, or modulating physiological neuron excitation. Typical neural stimulation comprises biphasic current-controlled charge-balanced pulses, with the second phase reversing the charge injection in the first phase. Commonly the first stimulation pulse phase is cathodic (electrons flow from the electrode to the tissue and the electrode potential becomes more negative) with the reverse pulse being anodic (opposite current flow with the electrode becoming more positive) (Merrill et al.; 2005; Cogan; 2008). Typical current-controlled waveforms are shown in figure 1E.

During stimulation, applied voltages exceed the small amplitudes required for the EIS assumption of pseudo-linearity; therefore, alternative characterisation methods are used. Cyclic voltammetry (CV) is a test of the current flow across the electrode interface due to Faradaic and non-Faradaic (capacitive) charge transfer as the electrode potential is cycled between two boundary values at a constant sweep rate ($V \cdot s^{-1}$). Typically, CV is conducted at a slow sweep rate, to achieve pseudo steady-state conditions. The resulting curve, or voltammogram (figure 1C), depends on the electrochemical reactions at the interface, reactant concentrations, reactant diffusion, the electrode area, electrode stability, and the potential sweep rate. Voltammograms may be normalised with respect to electrode area as a plot of current density against potential. CV allows the "background limits" to be determined, the potentials where anodic and cathodic currents flow due to the oxidation and reduction of the solute, termed the "water window" in aqueous solutions, depending on both the solution and the electrode material (Bard and Faulkner; 2001). Reactions occurring at the water window potential limits (oxidation and reduction of water) are irreversible because the products ($O_2$ gas and $H^+$ ions at the anodic limit and $H_2$ gas and $OH^-$ ions at the cathodic limit) do not all remain in

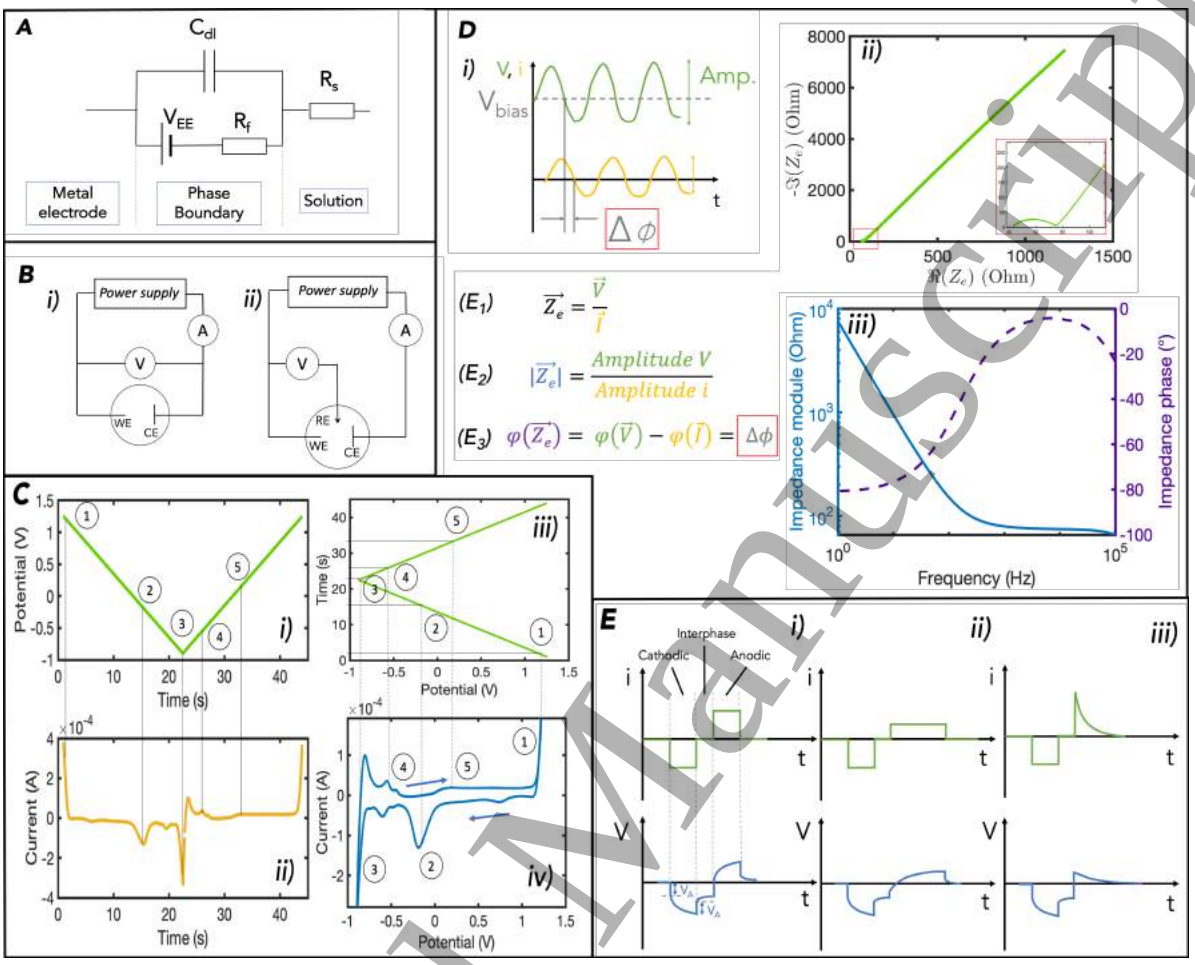


**Figure 1. Electrode-electrolyte model and characterisation techniques. A Equivalent electrical circuit of the electrode-electrolyte interface. B i) Two-electrode setup, B ii) Three-electrode setup. C cyclic voltammetry i) Potential sweep vs time, ii) Resulting measured current vs time, iii) Transposed potential sweep, iv) Cyclic voltammogram: current vs potential. D Electrochemical impedance spectroscopy i) Input voltage sine wave (green) and resulting current waveform (yellow), ii) Nyquist plot $\Im(Z_e)$ vs $\Re(Z_e)$, iii) Bode plot impedance module (equation $(E_2)$) and phase (equation $(E_3)$) vs frequency. E chronopotentiometry waveforms, examples of biphasic, cathodic-first, charge-balanced pulses i) symmetric, ii) asymmetric square anodic phase, iii) asymmetric capacitor discharge anodic phase.**

solution for the reverse reaction, and exceeding these limits will cause extremes of local pH (Brummer and Turner; 1975). Therefore the water window is commonly used as the hard limit of electrode potential for safe neural stimulation. In practice irreversible and harmful reactions may also occur within the water window (Merrill et al.; 2005; Boehler et al.; 2020; Cogan et al.; 2016).

CV allows the user to determine the available charge transfer reactions within the

water window. Peaks at potentials characteristic of faradaic reactions may be observed (1-5 in figure 1C). The observed current peaks are due to diffusion limiting reactions, where reactants at the electrode surface are exhausted and reaction rate depends upon the diffusion of reactants down a diffusion gradient from the bulk solution (Bard and Faulkner; 2001). The "background limits" are notable in not showing a diffusion limited peak, the solute (e.g. water) is readily available for the reaction at high concentration (1,3, in figure 1C).

CV enables the calculation of the charge storage capacity (CSC) of an electrode. Charge storage capacity (CSC) describes the amount of electric charge that can be "stored" during a full CV sweep, and is found by integrating the current-voltage curve with respect to time (Hudak et al.; 2017). CSC describes both cathodic and anodic charge transfer, commonly cathodic CSC (CSCc) is calculated for neural electrodes by taking the integral only when cathodic current is flowing (Boehler et al.; 2020). In practice during stimulation pulses the full CSC is not available, CV is measured using slow sweep rates to achieve pseudo steady-state unlike short stimulation pulses, and the electrode history and stimulation environment will act to obstruct and inhibit charge transfer (Hudak et al.; 2017).

The charge injection available during stimulation pulses is the charge injection capacity (CIC), or charge injection limit (CIL), of an electrode. Electrodes for neural stimulation should be able to safely inject a large charge per pulse, to ensure that neurons' activation thresholds can be overcome and physiological responses initiated (Geddes and Bourland; 1985). CIC is measured using practical stimulation pulses in current pulsing tests, typically with cathodic first, biphasic, current-controlled pulses where the anodic phase aims to achieve charge balance (figure 1E). For a given pulse width, pulse amplitude is increased until the amplitude is found at which the maximum electrode potential reaches either the cathodic or anodic background limit (Boehler et al.; 2020; Cogan; 2008). CIC is this maximum charge, for a given pulse width, at which electrolysis of water does not occur. To determine the potential across the phase boundary, the voltage drop due to the solution ($R_s$) must be excluded from the voltage response to a current pulse, either by accounting for the instantaneous potential change during pulse onset or with a pre-measured value for $R_s$. It must be noted that CIC measurements are not sufficient to determine safe charge injection limits for neural stimulation (Cogan et al.; 2016); however, the wide adoption of CIC means this is a useful comparator between electrodes.

### *1.2. Conductive Polymer Neural Electrodes*

Electrode properties are highly dependent upon electrode material choice. Noble metals are natural candidates for neural electrodes due to their high conductivity, ease of manufacture, and resistance to corrosion. Gold (Au), platinum (Pt) and iridium (Ir) are the most widely used metals for neural implants, along with alloys including PtIr and iridium oxide (IrOx). Increasing minaturisation to increase spatial

resolution and reduce tissue damage during implantation is reaching the technical limits of metal electrodes: smaller surface area leads to increased impedance and reduced CIC, degrading both recording and stimulation performance (Rossetti et al.; 2021; Aqrawe et al.; 2018). Furthermore metals' high Young's modulus leads to a mechanical mismatch between electrodes and the surrounding tissue. Mechanical mismatch causes relative micromotion and a longer lasting, more intense inflammatory response to the implant, increasing the distance to local neurons and degrading electrode performance (Axpe et al.; 2020; Liu et al.; 2020; Lacour et al.; 2016; Nguyen et al.; 2014; Stiller et al.; 2019, 2018; Vėbraitė and Hanein; 2021).

To overcome challenges with metal electrodes, conductive polymers coatings including polyaniline (PANI), polypyrrole (PPy), and poly (3,4)-ethylenedioxythiophene (PEDOT), have been investigated for their application to neural engineering (Wellman et al.; 2018; Akbar et al.; 2020). Conductive polymer coatings can improve implant integration by reducing Young's modulus, reduce electrode impedance by increasing $C_{dl}$, and increase CIC, improving stimulation and recording performance, and long-term stability (Guimard et al.; 2007; Cui and Martin; 2003; Venkatraman et al.; 2011; Simon et al.; 2016; Proctor et al.; 2016).

PANI takes one of three forms (pernigraniline, emeraldine and leucoemeraldine) depending upon oxidation state, with the half oxidized emeraldine form exhibiting the highest conductivity (Blinova et al.; 2008; Stejskal and Gilbert; 2002; Rossetti et al.; 2021). PANI has been used in scaffolds for neural regeneration and tissue engineering (Ghasemi-Mobarakeh et al.; 2011; Fan et al.; 2017; Garrudo et al.; 2019; Karimi-Soflou et al.; 2021). However, PANI has the highest conductivities only at low pH, which alongside processing challenges, has limited its use as a neural electrode coating (Blinova et al.; 2008; Rossetti et al.; 2021).

PPy is synthesised chemically or electrochemically by oxidation of pyrrole monomers (Akbar et al.; 2020; Vernitskaya and Efimov; 1997). The possibility of electrochemical synthesis means PPy is readily deposited as a coating on neural electrodes (Cui et al.; 2001). However, PPy electrode coatings are both brittle and undergo rapid delamination and loss of charge storage capacity following stimulation cycles, which is only reduced rather than prevented with co-coatings including carbon nanotubes and copper(I) (Lu et al.; 2010; Liu and Hwang; 2001; Yamato et al.; 1995).

### *1.3. Poly (3,4)-ethylenedioxythiophene (PEDOT)*

PEDOT is a conductive polythiophene polymerised from (3,4)-ethylenedioxythiophene monomers (EDOT, see figure 2). PEDOT polymer chains are not conducting in their native state, are insoluble in common solvents including water, are unstable undergoing rapid oxidation in air, and are not readily processed (Nardes; 2007; Sanchez-Sanchez et al.; 2019). To become conductive the PEDOT polymer backbone must be oxidised to its cationic form, achieved commercially using sodium persulfate oxidising agent (Groenendaal et al.; 2000). To balance the positively charged PEDOT a counter ion (or

"co-ion") is required. PEDOT co-ions include $Cl^-$, $SO_4^{2-}$, organic monomers such as p-toluenesulfonate (p-TS), organic polymers including poly(sodium 4-styrenesulfonate) (PSS), and biomolecules including albumin, heparin, and synthetic peptides (Ihalainen et al.; 2011; Harris et al.; 2012; Nardes; 2007; Rivnay et al.; 2016; Sanchez-Sanchez et al.; 2019). PEDOT with a PSS co-ion (PEDOT:PSS) is the most successful and widely used conductive polymer (Sanchez-Sanchez et al.; 2019) with applications including organic electrochemical transistors, organic electronic ion-pumps, organic light-emitting diodes, organic solar cells and neural electrode coatings (Lee et al.; 2017; Simon et al.; 2016). PSS anions act to support an aqueous dispersion of PEDOT:PSS (figure 3a,b), available commercially including as Clevios$^{TM}$ (formerly BAYTRON P) (Rivnay et al.; 2016; Groenendaal et al.; 2000). PEDOT:PSS films organise into a microstructure of PEDOT:PSS-rich grains within a hydrophilic, high-PSS concentration, phase (figure 3c), the grains can form locally crystalline or organised regions with closely stacked PEDOT:PSS lamellae (figure 3d) (Rivnay et al.; 2016; Hosseini et al.; 2020; Kim et al.; 2013). Films of PEDOT:PSS can be highly conductive (up to $4{\times}10^3\ S \cdot cm^{-1}$) and are more stable than PPy films (Worfolk et al.; 2015; Yamato et al.; 1995).

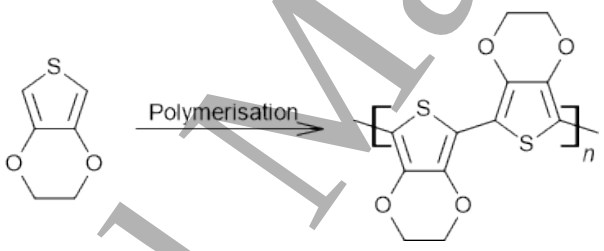


**Figure 2.** EDOT monomer (left) polymerises to form PEDOT (right). Not shown: co-ion or other synthesis details which are presented in (Groenendaal et al.; 2000) and (Nie et al.; 2021).

PEDOT:PSS and other conducting polymers exhibit mixed electronic/ionic conduction (Rivnay et al.; 2016; Sezen-Edmonds and Loo; 2017). Electronic conduction can occur along the polythiophene chain, by movement of positive polarons (positive charges or holes) arising from the charge due to PEDOT oxidation delocalised across a few EDOT monomers (Guimard et al.; 2007; Sezen-Edmonds and Loo; 2017). Conduction also occurs between PEDOT chain lamellae within grains by charge hopping and by interactions of stacked $\pi$-$\pi$ bonds (Hosseini et al.; 2020). Conduction of charge between PEDOT:PSS grains depends on the grain microstructure with high interconnectivity between conductive regions increasing conductivity (Hosseini et al.; 2020). Ionic conduction arises from the bulk movement of solvated ions into and within PEDOT:PSS from the solution or tissue (Rivnay et al.; 2016; Sezen-Edmonds and Loo; 2017).

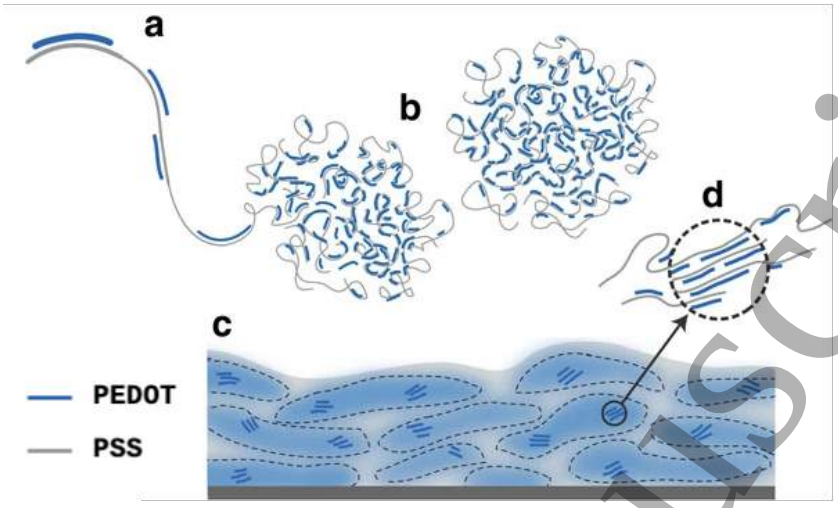


**Figure 3.** Schematic of PEDOT:PSS coating microstructure through solution processing, modified from CC-BY-4.0 Rivnay et al. (2016). PEDOT chains polymerise on PSS (a), form an entangled structure in suspension (b), which precipitates on the electrode surface forming PEDOT-rich grains inside insulating PSS walls (c). PEDOT-rich high conductivity grains are highlighted in d.

### *1.4. Methods of PEDOT Deposition*

PEDOT coatings and electrodes may be formed through a range of processes (Kitto et al.; 2019). The focus of this review is PEDOT coating electrodeposition, in this section we will briefly review the variety of methods reported for PEDOT processing.

Electrodeposition is typically carried out in a three electrode cell (figure 1B) with deposition occurring at the positively biased working electrode when the electrode potential exceeds the potential for EDOT oxidation (Guimard et al.; 2007; Subramanian and Martin; 2021). Electrodeposition may be carried out by one of three common methods: potentiostatic (PS) deposition, where electrode potential is held constant, potentiodynamic (PD) deposition, where electrode potential is varied usually linearly or cyclically, for instance in cyclic voltammetry (CV), galvanostatic (GS) deposition, where electrode current is held constant, and galvanodynamic (GD) deposition where electrode current is varied with time in a controlled manner (Sanchez-Sanchez et al.; 2019; Kitto et al.; 2019).

During PEDOT electrodeposition, EDOT monomers at the working electrode are oxidised to highly reactive radical cations. The radical cations condense to dimers, trimers, and longer oligomers in a process of electropolymerisation (Sanchez-Sanchez et al.; 2019; Subramanian and Martin; 2021). Oligomers nucleate on the working electrode and precipitate as the chain length increases becoming insoluble PEDOT chains of between 6 and 20 EDOT monomers (Nardes; 2007; Sanchez-Sanchez et al.; 2019; Kim et al.; 2021). The EDOT nucleation sites merge and coalesce forming a film of PEDOT at the electrode, with the film forming initially at the electrode edges where charge density is highest (Subramanian and Martin; 2021; Liu et al.; 2015). At

the electrode PEDOT is also oxidised to a positively charged cation as the chain is polymerised because the potential for oxidation falls as chain length increases and is lower (between +0.55 V and +0.1 V vs Ag|AgCl reference) than the potential already required for EDOT oxidation (at least +0.85 V vs Ag|AgCl), this PEDOT cation charge is balanced by co-ions which co-deposit from solution to balance the charges (Subramanian and Martin; 2021; Guimard et al.; 2007; Sanchez-Sanchez et al.; 2019; Pigani et al.; 2004). Thus electrodeposition selectively coats the working electrode even on complex non-planar surfaces, and can achieve very thin PEDOT films of tens to hundreds of nm (Guimard et al.; 2007).

In addition to forming layers at surfaces electrodeposition can form conductive fibres and microwires of PEDOT between the tips of sharp electrodes or with controlled electrodeposition conditions (Thourson and Payne; 2017; Morris et al.; 2017; Eickenscheidt et al.; 2019). Electropolymerisation can also be carried out *in situ* within hydrogels immersed in EDOT:co-ion solutions (Bhat et al.; 2021; Fu et al.; 2021; Wang et al.; 2019; Akbar et al.; 2020), *in vitro* within tissue cultures (Chen et al.; 2022), and *in vivo* within the tissue surrounding an electrode following local injection of EDOT:co-ion solution (Murbach et al.; 2018; Ouyang; 2014; Ouyang et al.; 2011), forming an interpenetrating conductive polymer within the hydrogel or tissue with the highest concentration adjacent to the electrode.

Solution processing forms PEDOT films or coatings from PEDOT:co-ion suspensions, mixtures, and solutions. Spin coating (or spin casting) forms a uniform thin film from a viscous PEDOT:co-ion suspension on a flat substrate by rotating the substrate to spread the PEDOT suspension by centrifugal force (Kitto et al.; 2019; Rossetti et al.; 2021). Spin coated PEDOT films may be patterned by planar photolithography (Lee et al.; 2017; Donahue et al.; 2018; Cea et al.; 2020; Dijk et al.; 2022). However, spin coating is limited to planar surfaces (Rossetti et al.; 2021). Dip coating can coat more complex 3-dimensional surfaces by dipping a sample into a PEDOT:co-ion suspension, but is challenging to selectively pattern (Proctor et al.; 2018). Drop casting PEDOT:co-ion suspensions can achieve selective coatings (Leleux et al.; 2013); however drop cast PEDOT coatings have shown poor adhesion to metal electrode substrates (Benoudjit et al.; 2018). Solution processed PEDOT may have added cross-linkers for stability (Zhang et al.; 2015; Sordini et al.; 2021), additives to control PEDOT self-assembly (Dauzon et al.; 2019; Cheng et al.; 2022; Wang, Wang, Zhu, Wang, Gao, Gao and Gao; 2021; Han and Foulger; 2006; Huang et al.; 2017), and dopants for conductivity enhancement (Ouyang; 2013; Gueye et al.; 2016; Wang et al.; 2017; Shahrim et al.; 2021). Solution processing can form conductive hydrogels including directly from hydrogel precursor and PEDOT:co-ion mixtures (Ren et al.; 2021; Gotovtsev et al.; 2019; Zhang et al.; 2020; Furlani et al.; 2022; Akbar et al.; 2020), and by re-swelling pre-cast hydrogels in conductive polymer solutions (although re-swelling is rarely used for PEDOT containing hydrogels) (Bhat et al.; 2021).

To enhance mechanical and structural properties of PEDOT films, nanoparticles such as silica nanoparticles (Woeppel et al.; 2019), metallic nanoparticles (Xu et al.;

2022), graphene oxide (Luo et al.; 2013) and carbon nanotubes (CNTs) (Chen et al.; 2013; Castagnola, Maiolo, Maggiolini, Minotti, Marrani, Maita, Pecora, Angotzi, Ansaldo, Boffini, Fadiga, Fortunato and Ricci; 2015; He et al.; 2021; Lu et al.; 2021) can be embedded between polymer chains during solution processing or electrodeposition to form a nanocomposite. Nanoparticles form non-covalent bonds with PEDOT to increase mechanical stability and film flexibility (Adekoya et al.; 2021), and may promote neuron differentiation and neurite growth on PEDOT nanocomposite films (Depan and Misra; 2014).

PEDOT solutions may also be processed by printing in 2- or 3-dimensions. Screen printing patterns PEDOT:co-ion films by printing onto a 2D substrate through a mesh screen covered with a negative mask. PEDOT suspension viscosity is important to achieve a printable formulation which does not flow once transferred to the substrate, dimethyl sulfoxide (DMSO), Triton X-100, methyl cellulose, and poly(dimethylsiloxane-b-ethylene oxide) have been added to achieve appropriate screen printing rheologies (Sinha et al.; 2017; Tseghai et al.; 2020; Niu et al.; 2021).

3D printing forms 3-dimensional PEDOT structures using PEDOT suspensions with rheology tailored to allow extrusion while retaining structure following printing. High concentration suspensions (7% PEDOT:PSS) (Yuk et al.; 2020), cross-linking agents (Heo et al.; 2019; Aggas et al.; 2020; Abdullah and Phairatana; 2022; Tomaskovic-Crook et al.; 2019), additives and copolymers for melt-extrusion (Li et al.; 2021; Dominguez-Alfaro et al.; 2021), and thixotropic additives (Rastin et al.; 2020) have been used to achieve 3D printable PEDOT formulations. Cell-laden conductive printing inks have been achieved for direct printing of conductive PEDOT scaffolds containing living cells (Rastin et al.; 2020).

Conductive fibres containing PEDOT may be formed by electrospinning, extruding a PEDOT:co-ion suspension under a high voltage electric field to form fibres which are collected on a substrate (Xue et al.; 2019; Kitto et al.; 2019). Optimised formulations including carrier polymers such as poly(vinyl alcohol) (PVA), Polycaprolactone (PCL) and poly(ethylene oxide) (PEO) are used to achieve electrospinnable PEDOT:co-ion mixtures (Bessaire et al.; 2017; Babaie et al.; 2020; Ritzau-Reid et al.; 2020; Lerond et al.; 2022), and conductivity enhancers including silver nanoparticles and graphene oxide may be added (Ngoensawat et al.; 2022; Liu et al.; 2022). Electrospinning can form conductive, porous, fibrous lattices for tissue engineering (Babaie et al.; 2020; Ritzau-Reid et al.; 2020), and additional PEDOT coatings may be electropolymerised onto conductive fibres after electrospinning (Zubair et al.; 2016).

Given the advantages offered by electrodeposition for miniaturised neural electrodes, this review focusses on electrodeposited PEDOT. Electrodeposited PEDOT coating structure is influenced by deposition methods including deposition charge, co-ion, and substrate surface state. Coating structure and morphology play a substantial role in PEDOT coating electrochemical performances. Therefore, electrodeposition parameters directly influence PEDOT coating structure and electrochemical performance. However, the range of deposition parameter combinations previously investigated by individual

studies has not been comprehensively compared with respect to deposition outcomes. This review will highlight these relationships between electrodeposition parameters, and PEDOT coating electrochemical performance.

## 2. Material and Methods

### *2.1. Search Strategy*

A semi-systematic literature search was conducted. The following five electronic literature databases were used: Google Scholar, IOPscience, PubMed, Web of Science, and ProQuest Dissertation & Theses Global. A comprehensive list of search keywords was developed including: poly (3,4)-ethylenedioxythiophene, PEDOT, coating, performance, neural, nerve, interfaces, stimulation, recording, electrode, electrodeposition. Search terms were combined into queries to allow for synonyms, e.g. "PEDOT AND neural OR nerve AND electrode".

### *2.2. Study Selection*

Studies were considered for inclusion by one reviewer. Where the reviewer did not reach a conclusion on study relevance a second, and third reviewer opinion was sought.

Inclusion criteria were studies of **electrodeposited** PEDOT coatings deposited **in vitro** on **metallic substrates** for the purposes of **neural interfaces and neural engineering**. Studies were excluded for reasons including: PEDOT was **spin-coated, cast, or deposition with another non-electrodeposition method**; electropolymerisation was carried out **in vivo**; or deposition on **non metallic substrates**, except when the substrate itself was deposited on metallic electrodes (e.g. adhesion coatings).

### *2.3. Data Extraction and Analysis*

Study data was extracted by a single reviewer, and checked by a second reviewer. Study data was tabulated, and where information differed between studies, units were harmonised and common parameters were calculated. Where appropriate, area normalised values were calculated to facilitate direct comparison between studies. Analysis was carried out using MATLAB (R2020A, The Mathworks) on Windows 10 and MacOS (Big Sur) to sort data and generate comparative figures.

We considered a wide scope of materials and methods for deposition and characterisation. A summary of extracted data is presented in table 1. Two sets of methods were reviewed separately: electrodeposition methods (section 3.1), which influence the coating performance directly, and characterisation methods (section 3.2), which determine how performances are reported. Influence of deposition protocol on coating morphology was investigated (section 3.3), and electrochemical performance was reviewed across three key measures: impedance (section 3.4), charge storage capacity (3.5), and charge injection limit (3.6).

**Table 1.** List of extracted study data.

| | |
|---|---|
| **Summary** | DOI; Authors; Date; Application[1]. |
| **Deposition** | Substrate; Geometry[2]; Pretreatment[3]; Cleaning; Monomer; Counter-Ion; Solution; Electrodes; Mode; Deposition Charge. |
| **Characterisation** | Morphology Imaging; Characterisation Environment; Characterisation[4] Parameters. |
| **Performance** | Impedance; Charge Storage Capacity; Charge Injection Capacity. |

[1] Application includes the role of the PEDOT coated interface, e.g. for recording or stimulation.
[2] Geometry includes geometric surface area and dimensions used to normalise extracted values.
[3] Pretreatment includes roughening, polishing, and pre-deposition.
[4] Mechanical and electrochemical characterisation.

## 3. Results

### *3.1. PEDOT coating electrodeposition materials and methods*

In this section we highlight the most common choices for PEDOT electrodeposition materials and methods, the effects of materials and methods on electrode performance is discussed in subsequent sections. PEDOT electropolymerization is influenced by choices of materials and methods, which have been linked to structural features of the coating or directly to the electrochemical performance of the coated electrode: for example, the substrate surface state and EDOT:co-ion ratio influence coating quality and stability (Tamburri et al.; 2009; Aqrawe et al.; 2019). Results are presented in plots showing deposition materials and methods combinations (figures 4 and 5), and detailed numerical results are presented as tables in the appendix, (section 4).

The most common electrode substrates are gold and platinum (figure 4, table 2). Textured platinum or gold nanoparticles are also used to provide a rough substrate and promote coating adhesion (Green et al.; 2012; Boehler et al.; 2017; Lee et al.; 2018; Krukiewicz et al.; 2019).

Poly(styrene sulfonate) (PSS) is the most common co-ion for PEDOT electrodeposition (figures 4, 5 and table 3). PSS was the first to be used (Guimard et al.; 2007), and has been studied most extensively. Perchlorate ion ($ClO_4$) and p-toluenesulfonate (pTS) are widely used in recent studies; co-ion choice allows users to modify the coating performance (see sections 3.5, 3.6). PSS and pTS interact with EDOT, templating the structure as shown in figure 3, while smaller, more mobile co-ions such as $ClO_4$ or tetrafluoroborate ($BF_4$) insert themselves between PEDOT chains as a charge balancing dopant (Kayinamura et al.; 2010). Peptides and biomolecules including albumin, heparin, and glutamate have also been used as co-ions to improve implant integration in vivo (table 3).

GS and PS deposition are the most common modes (figure 4, table 4). Twice as many studies used GS compared to PS deposition, which resulted in four times as many results (entries), showing that GS deposition mode is more widely characterised than

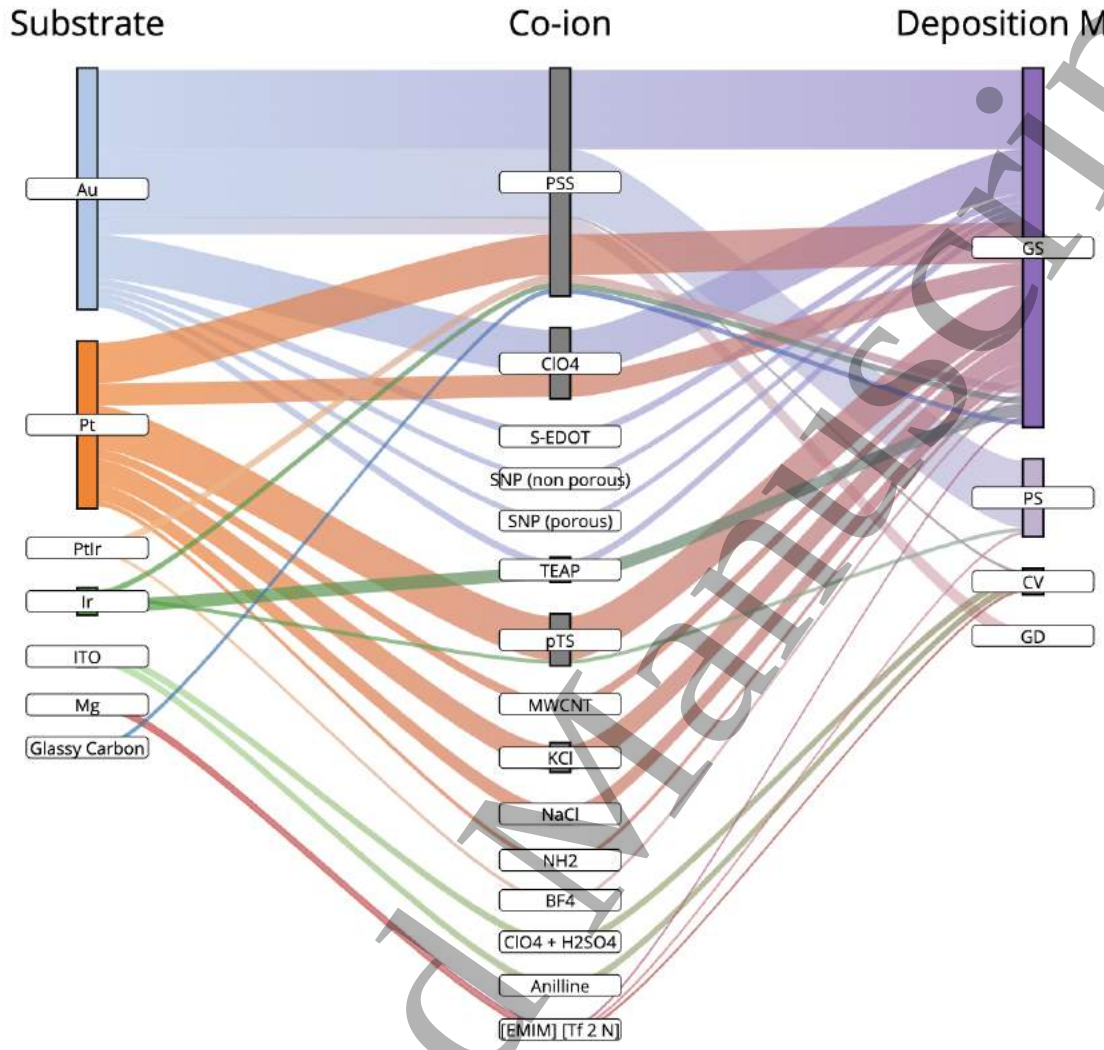


**Figure 4.** Alluvial plot of substrate prevalence, co-ion and deposition mode choice. Options with fewer than three entries are not shown. Complete lists of references and numbers of studies are tabulated in the appendix for: substrates, table 2; co-ions, table 3; and deposition mode, table 4. Abbreviations are as follows: Au, gold; Pt, platinum; PtIr, platinum/iridium alloy; Ir, iridium; ITO, indium tin oxide; Mg, magnesium; PSS, poly(sodium 4-styrenesulfonate); $ClO_4$, perchlorate ion; S-EDOT, sulfonatoalkoxy EDOT; SNP, silica nanoparticles; TEAP, tetraethylammonium perchlorate; pTS, p-toluenesulfonate; MWCNT, multi-walled carbon nanotubes; $KCl$, potassium chloride; $NaCl$, sodium chloride; $NH_2$, azanide anion; $BF_4$, tetrafluoroborate; $H_2SO_4$, sulfuric acid; [EMIM][Tf2M], 1-Ethyl-3-methylimidazolium bis(trifluromethylsulfonyl)imide; GS, galvanostatic; PS, potentiostatic; CV, cyclic voltammetry; GD, galvanodynamic.

PS. Galvanodynamic (GD) deposition often consists of a current ramp applied until a target current is reached and maintained constant for the rest of the deposition. Cyclic Voltammetry (CV) is also used as a potentiodynamic deposition method. The majority of studies performed deposition (and electrochemical measurements) in a three-electrode cell.

Less common deposition materials and methods choices are often linked to a single item in the other categories. For instance as shown in figure 4, the substrate glassy carbon has only been paired with the co-ion PSS and the deposition mode GS. While the most frequent co-ion (PSS) is paired with a wide range of materials and methods, $ClO_4$ and pTS tended to be predominantly paired with the same set of materials and methods choices. For example pTS was almost exclusively deposited galvanostatically on platinum and $ClO_4$ was solely deposited galvanostatically. This shows clear knowledge gaps in the complex multi-factorial process of PEDOT electrodeposition, where possible combinations have not been investigated or reported.

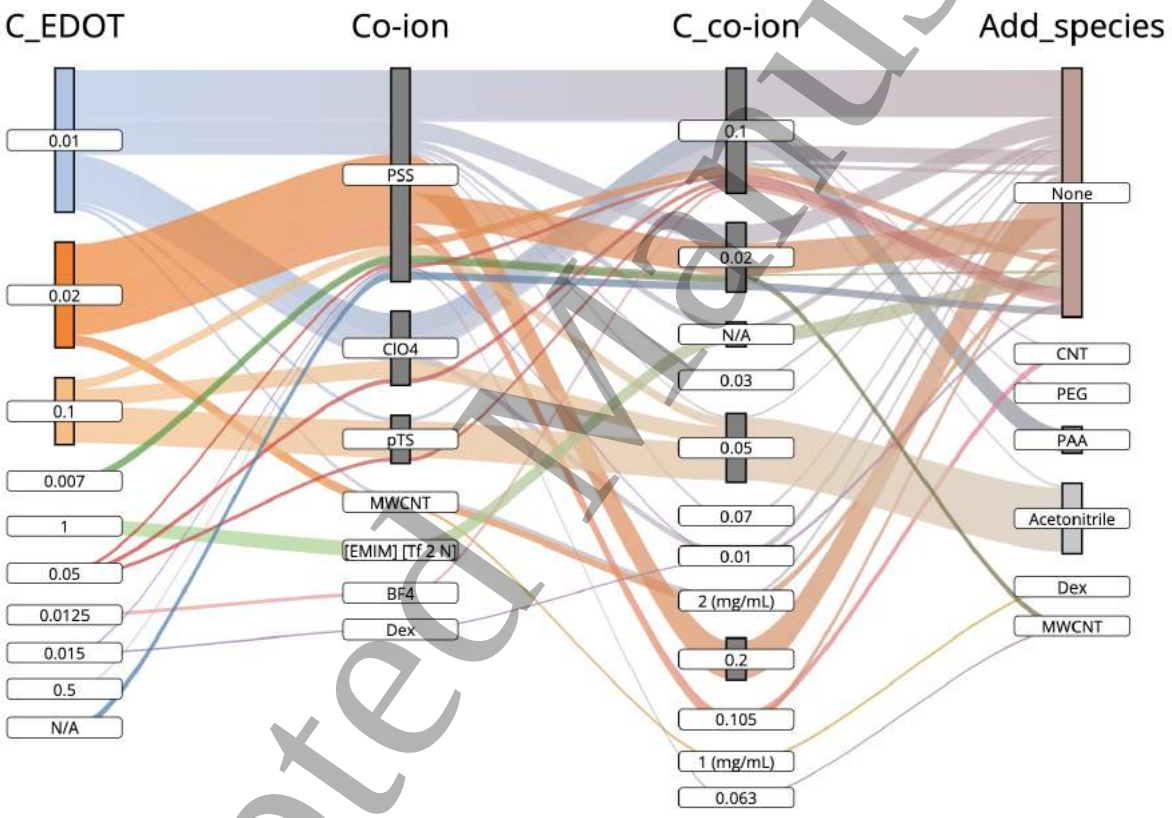


**Figure 5.** Alluvial plot representing choices of EDOT concentration (C_EDOT), co-ion, co-ion concentration (C_co-ion) and additional species added to the coating solution (Add_species)

. Options with fewer than two entries are not shown. Concentrations are given in M (mol/L), unless otherwise specified. Complete lists of references and numbers of studies are tabulated in the appendix for: EDOT concentration, table 6; co-ion, table 3; and co-ion concentration, table 5. Abbreviations are as follows: PSS, poly(sodium 4-styrenesulfonate); $ClO_4$, perchlorate ion; pTS, p-toluenesulfonate; MWCNT, multi-walled carbon nanotubes; $BF_4$, tetrafluoroborate; Dex, dextran; CNT, carbon nanotubes; PEG, polyethylene glycol; PAA, poly(acrylic acid).

PSS, the most popular co-ion, also had the greatest variation in reported

concentration, from 0.01 M to 0.29 M, with most studies using 0.1 M or 0.02 M PSS (figure 5, table 5). Less variability is present in reported concentration of less popular co-ions. $ClO_4$ is mostly used at 0.1 M, and pTS is mostly used at 0.05 M. Multi walled carbon nanotubes' (MWCNT) molar mass is not well defined, therefore MWCNT concentration is reported as mass concentration (1 mg/mL to 2 mg/mL table 5).

EDOT monomer is used in a vast majority of studies at a concentration of 0.01 M (48% of studies) and 0.02 M (21%) (table 6). Most often, the EDOT:co-ion ratio was 1:10; 1:2 and 1:1 were also frequent (figure 5). Amongst the major co-ions, pTS and a fraction of $ClO_4$ studies had a 2:1 EDOT:co-ion ratio. As expected, most studies did not use additional species in deposition. Acetonitrile was listed as an additional species in this table, as it can have possible effects on deposition. However acetonitrile was not deposited as another component of the polymer matrix but used as a solvent or solvent component to aid EDOT solubility.

Only 30% of studies specified a substrate cleaning method before electrodeposition. The most common cleaning method was CV cycling in $H_2SO_4$ or PBS. A single study specified not cleaning the substrate prior to deposition (Castagnola, Descamps, Lecestre, Dahan, Remaud, Nowak and Bergaud; 2015).

After electrodeposition 44% of studies report cleaning the PEDOT coated sample. The most common cleaning protocol is rinsing PEDOT coated samples with deionised water to remove unpolymerized monomer, and air drying. Other post-deposition protocols include: rinsing with dichloromethane (Yang et al.; 2005; Abidian et al.; 2006; Ludwig et al.; 2006; Abidian et al.; 2007; Abidian and Martin; 2008; Abidian et al.; 2009; Abidian and Martin; 2009), sonication (Sebaa et al.; 2013), and applying a few CV cycles in a cleaning solution (Mandal et al.; 2014, 2015; Pranti et al.; 2018). Post-deposition protocols used for organic electronics to improve PEDOT conductivity, including acid treatment, thermal treatment, UV irradiation, polar organic solvent addition, and surfactant treatment, are not widely reported in the neural engineering literature (Shi et al.; 2015). This may be due due to concerns with toxicity, compatibility with other implant materials, and reduced coating stability.

### *3.2. PEDOT coating characterisation methods*

Observed electrochemical performance depends upon the test conditions used: the test solution and parameters. This section summarises methods of morphological, mechanical, and electrochemical characterisation, including test parameters for electrochemical impedance spectroscopy (EIS), cyclic voltammetry (CV), and chronopotentiometry (CP), used to investigate the performance of PEDOT-coated neural interfaces. The characterisation method parameters used in the considered studies are summarised in the appendix.

#### *3.2.1. Imaging methods*

Coating morphology was evaluated most commonly using scanning electron

microscopy (SEM). SEM imaging consists in sending an electron beam to the sample and capturing the reflected electrons to get a black and white contrast image of structure and conductivity. Magnification and accelerating voltage (in kV) are the most commonly reported parameters.

For quantitative measurements of thickness and roughness, more precise techniques including focussed-ion beam (FIB) and atomic force microscopy (AFM) were preferred. FIB can be operated in two modes: high current FIB, which is a destructive method creating a transversal cut though a sample, and low current FIB, which is a non-destructive imaging method similar to SEM. Both FIB modes can be used to image coating thicknesses. AFM is a high resolution method, where a flexible cantilever head reflects a laser signal to a photodiode. The head can either be force-controlled (tapping mode), where the head keeps a constant distance with the substrate surface, measuring roughness through the variation of photodiode current, or current-controlled (contact mode), where the head's position is kept steady and electron exchange with the substrate via tunnelling effect generates a conductivity map of the substrate. AFM spring constant (N/m) and resonant frequency (Hz) are important parameters to report.

### *3.2.2. Mechanical testing*

Mechanical testing primarily tested coating adhesion. The tape test consists in attaching a calibrated tape strip to the coating, exerting a 180° pull, and measuring the force required for coating delamination. Another adhesion test reported involved sonicating samples in deionized water until delamination was observed; however, this method is less quantifiable and reproducible.

### *3.2.3. Electrochemical impedance spectroscopy methods*

Electrochemical impedance spectroscopy (EIS) parameters used to characterise PEDOT coated neural electrodes are given in figure 15 and tables 7 and 8 (see appendix). A wide frequency range enables a more thorough characterisation of the electrode and can allow for calculation of characteristic parameters including solution resistance ($R_s$), obtained at high frequencies ($>$ 10 kHz), and double layer capacitance ($C_{dl}$). The most common EIS frequency range is 1 Hz to 100 kHz and the majority of EIS ranges were centered at 100 Hz to 1 kHz, within a typical biosignal recording bandwidth (figure 15, appendix).

EIS amplitude (table 7) relates to the amplitude of the AC excitation potential used as input. Over 60% of studies used EIS amplitudes $\leq$ 10 mV. Small amplitudes are usually recommended to maintain the assumption of linearity and we can see in table 7 that this requirement is respected in most studies (Boehler et al.; 2020).

EIS potential is the voltage at which the working electrode is held with respect to the reference electrode; it is the average value of the AC voltage applied. Most studies do not state EIS potential, we assume that EIS was carried out at open-circuit potential (OCP) but we cannot be sure. A few studies performed EIS at potentials which do not correspond to a reported OCP. Characterisation may then not reflect electrode

behavior in operating conditions (Bobacka et al.; 2000; Peng et al.; 2007; Harris et al.; 2012; Ouyang et al.; 2017; Qu; 2017; Bodart et al.; 2019; Popov et al.; 2019).

The choice of electrochemical measurement parameters may be strongly influenced by available equipment and default parameters. For example, the default parameters for the potentiostat equipment present in our laboratory include: 0.2 Hz to 100 kHz frequency range, 10 mV RMS AC amplitude, DC voltage: 0 V vs OCP.

### *3.2.4. Cyclic voltammetry methods*

Cyclic voltammetry parameters used to characterise PEDOT coated neural electrodes are given in figure 16 and table 9 (see appendix). As for EIS, the voltage ranges used for CV were plotted from largest to smallest. The most common ranges are [-0.6, +0.8] and [-0.9, +0.5] vs Ag|AgCl, which correspond respectively to the water windows for Pt/PtIr and for PEDOT (Cogan et al.; 2016).

The sweep rate describes the change in applied working electrode potential with time. The most commonly chosen sweep rate is 100 mV/s. A fast sweep rate (500 mV/s and above) considers fast electron transfers and mostly capacitive charge injection, while a slow sweep rate (50 mV/s and below) is intended to allow reactions to reach pseudo-steady-state and will be more sensitive to faradaic charge injection (Harris et al.; 2018).

### *3.2.5. Current pulsing methods*

The majority of current pulsing studies used cathodic first (CF), current-controlled biphasic pulses, which is the recommended standard for stimulation (Merrill et al.; 2005) (table 10). The pulse width was variable, with most studies using pulse widths in the 100's of $\mu$s range and with the most common pulse widths at 100 $\mu$s, 200 $\mu$s, 500 $\mu$s and 1000 $\mu$s (table 11). A single study used long pulses of 60 s to study polarization over longer time scales (Bobacka; 1999). Interpulse delays were not mentioned in most studies, and where they were described, the durations varied (table 12).

## *3.3. Coating morphology*

PEDOT electrodeposition materials and methods control the macroscopic and microscopic structure of PEDOT conductive coatings. Factors including co-ion choice and deposition charge affect different steps of the polymer growth, and can yield smooth and compact, or rough and porous coatings. PEDOT coating morphology has been directly linked to electrochemical performance: increased roughness increases real electrode surface area, decreasing electrode impedance (Boehler et al.; 2020). Therefore, analysis of coating morphology will hint at the electrochemical behavior of electrodes, addressed later in this review.

The range of electrodeposited PEDOT coating morphologies on planar neural electrodes is shown in figure 6. The typical granular or "cauliflower" morphology of PEDOT coatings (figure 6 C,I,K.) arises from a 2D-3D growth process (Tamburri et al.; 2009; Castagnola et al.; 2014; Chapman et al.; 2018; Pingree et al.; 2008).

PEDOT nuclei precipitate on the electrode and grow by polymer chain extension on the electrode surface, which is the 2D growth phase. When adjacent nuclei overlap 3D growth commences, forming a bulk structure with PEDOT nuclei distributed throughout conduction dots (Pingree et al.; 2008). Increased charge density at electrode edges causes thickening of coatings at the edge of planar electrodes where PEDOT nuclei are more likely to precipitate (figure 6A-E) (Liu et al.; 2015; Subramanian and Martin; 2021).

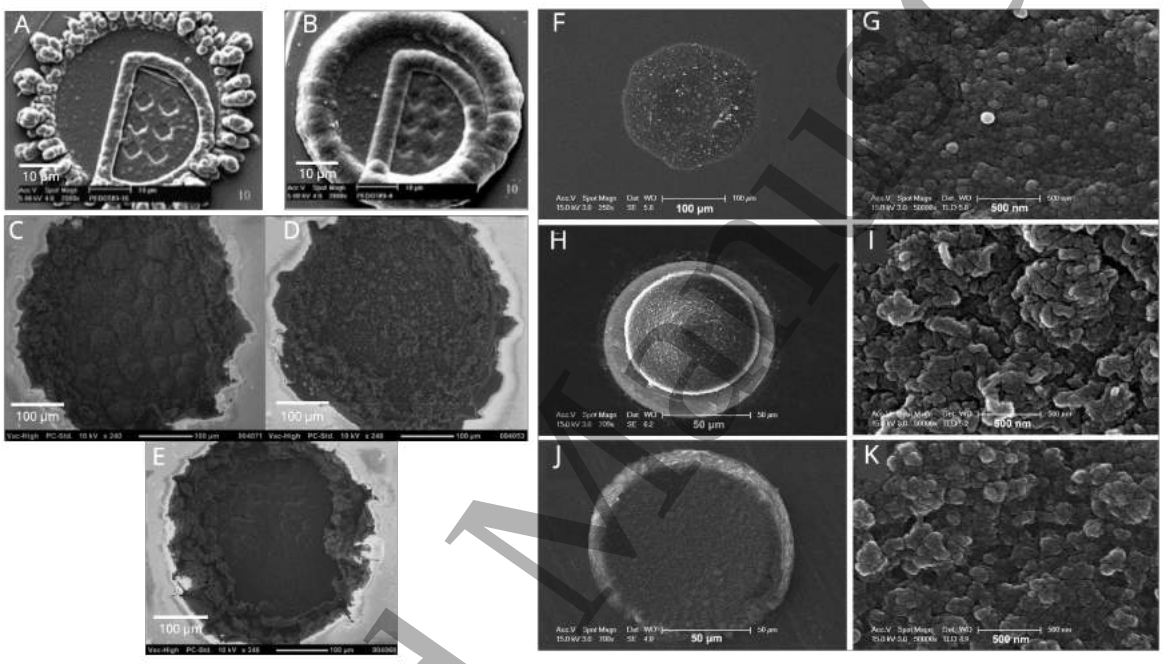


**Figure 6.** A and B: PS and GS depositions (Cui and Martin; 2003); C, D and E: GS deposited with pTS, $ClO_4$ and PSS (Green et al.; 2012); F, H and J: morphology of PS deposited PEDOT:MWCNT, GS deposited PEDOT:MWCNT and GS deposited PEDOT:PSS; and G, I and K show the respective microscopic structure (Zhou et al.; 2013). Figures modified or reproduced from: Chapman et al. (2018) CC-BY-3.0; Cui and Martin (2003) reprinted from Sensors and Actuators B: Chemical, Vol 89, Cui and Martin, "Electrochemical deposition and characterisation of poly(3,4-ethylenedioxythiophene) on neural microelectrode arrays", Pages 92-102, Copyright (2003), with permission from Elsevier; Castagnola et al. (2014) reprinted from Synthetic Metals, Vol 189, Castagnola et al., "Morphology and conductivity of PEDOT layers produced by different electrochemical routes", Pages 7-16, Copyright (2014), with permission from Elsevier; Green et al. (2012) reprinted from Biomaterials, Vol 33, Green et al., "Substrate dependent stability of conducting polymer coatings on medical electrodes", Pages 5875-5886, Copyright (2012), with permission from Elsevier; Zhou et al. (2013) reprinted from Acta Biomaterialia, Vol 9, Zhou et al., "Poly(3,4-ethylenedioxythiophene)/multiwall carbon nanotube composite coatings for improving the stability of microelectrodes in neural prostheses applications", Pages 6439-6449, Copyright (2013), with permission from Elsevier.

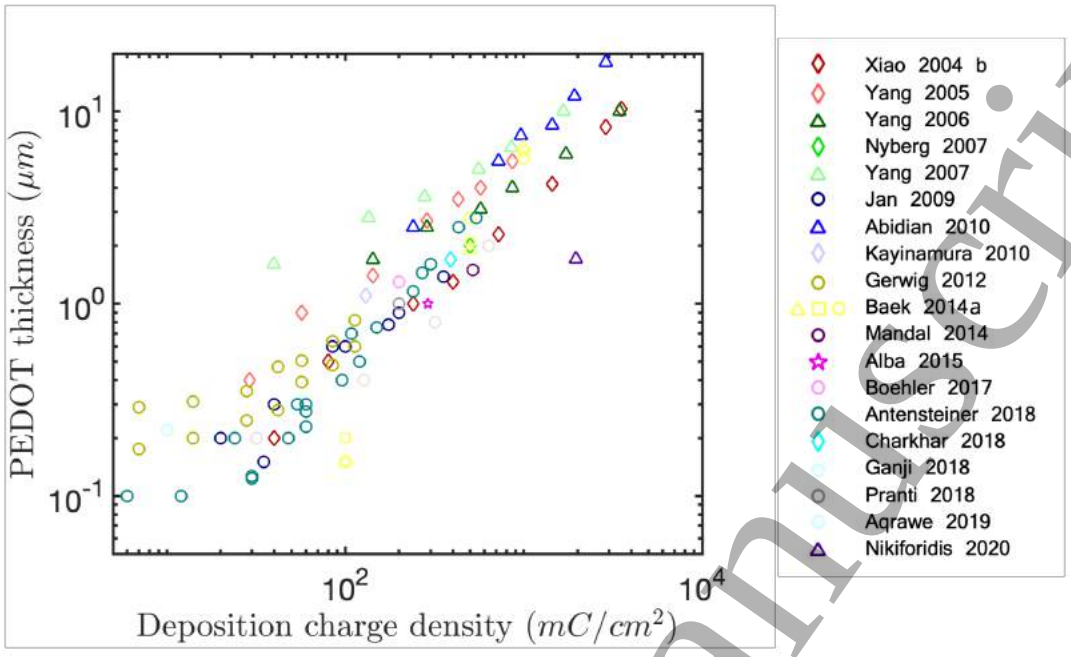


**Figure 7.** PEDOT coating thickness versus deposition charge density. Co-ions are indicated by marker shape: ○ for PSS, Δ for $ClO_4$, □ for pTS, ⋆ for MWCNT and ◊ for other species.

*3.3.1. Thickness*

The effect of deposition materials and methods on PEDOT thickness was monitored in 19 studies. Increasing deposition charge density increases PEDOT coating thickness (figure 7). At charge densities above 30 $mC/cm^2$ PEDOT coating thickness is positively correlated with deposition charge density: increased charge density leads to increased coating thickness (0.0367 $\mu$m per $mC/cm^2$ or 36.7 $\mu$m per $C/cm^2$). This relationship is visually consistent between studies despite different deposition conditions and electrode characteristics (figure 7) (Xiao, Cui and Martin; 2004; Yang et al.; 2005; Yang and Martin; 2006; Yang et al.; 2007; Abidian et al.; 2010). At low charge densities, below 30 $mC/cm^2$ the correlation deviates from linear: thickness remains low and does not appear to correlate with charge density (Gerwig et al.; 2012; Antensteiner; 2018).

We note differences from the global trend in a few studies. Yang et al. (2007) shows a shallower linear trend. The initially higher thickness may be due to deposited PEDOT nanofibrils, using polyacrylic acid (PAA) as a solvent. Increasing deposition charge density increased thickness only slightly. Some studies report several thicknesses for identical deposition charge densities (Baek et al.; 2014a; Gerwig et al.; 2012; Antensteiner; 2018), due to other differences in deposition method. Addition of CNT results in consistently thicker coatings (Gerwig et al.; 2012). Baek et al. (2014a) used PSS, pTS and $ClO_4$ as co-ions but no clear relationship between co-ion choice and coating thickness was observed. Antensteiner (2018) used different deposition

current×time pairs to achieve similar charge densities: no clear trend in the effect of current density or time was apparent which was not explained by the resulting charge density.

### *3.3.2. Roughness*

PEDOT coatings have a rough surface and may incorporate porosity as well. Therefore, the surface available for electrochemical interaction is increased. Two metrics are distinguished to describe surface area: geometric surface area (GSA) for the substrate dimension, and real surface area (RSA) for the apparent surface available for electrochemical interactions accounting for roughness and porosity.

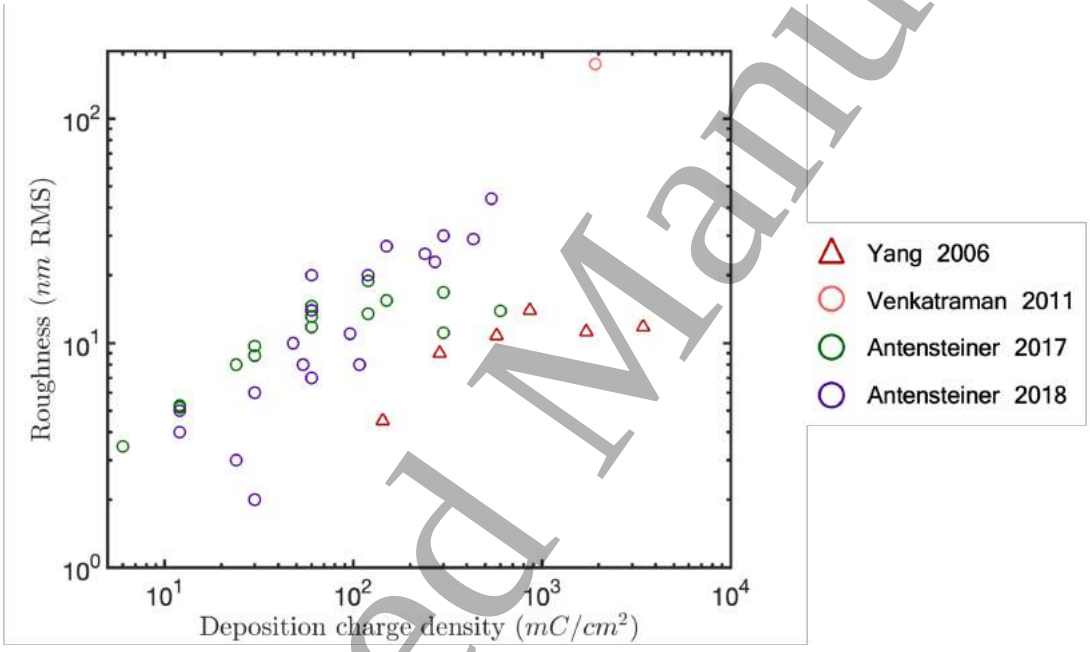


**Figure 8.** PEDOT coating roughness versus deposition charge density. Co-ions are indicated by marker shape: ∘ for PSS, Δ for $ClO_4$, □ for pTS, ⋆ for MWCNT and ◊ for other species. Roughness in root mean squared (RMS) average of deviation from the mean profile height.

PEDOT coating roughness was reported in 4 studies (Yang and Martin; 2006; Venkatraman et al.; 2011; Antensteiner and Abidian; 2017; Antensteiner; 2018). Antensteiner and Abidian (2017) and Yang and Martin (2006) observed linear increases in roughness with deposition charge density before reaching a plateau at approximately $R_a = 10\ nm$, where increasing deposition charge density does not increase coating roughness further (figure 8). Antensteiner (2018) observed a linear correlation between roughness and charge density across all roughnesses. Venkatraman et al. (2011) calculated coating roughness from a theoretical model (following Cui and Martin (2003)), and although this follows the global linear trend this observation must be considered with caution because: roughness was not directly measured; and the reported roughness

is approximately 4 times larger than other observed roughnesses. The length scale dependence of surface roughness measurements makes interpretation between studies challenging where the cut off lengths are unknown.

Antensteiner (2017; 2018) varied the deposition charge density with both current density (figure 9 A) and deposition time (figure 9 B); therefore similar charge densities may result from different current density and time combinations. Longer deposition times correlated with rougher coatings (figure 9 A.), approaching a plateau in Antensteiner and Abidian (2017). Increased current density also correlated with rougher coatings (figure 9 B), but with maxima observed at similar charge densities (600 s and 300 s depositions have peak roughness at 120 mC/cm$^2$ and 150 mC/cm$^2$ respectively) in Antensteiner and Abidian (2017). Similar trends in Antensteiner (2018) are less consistent, attributable to the increased edge effect of smaller electrodes and underlying electrode surface variation.

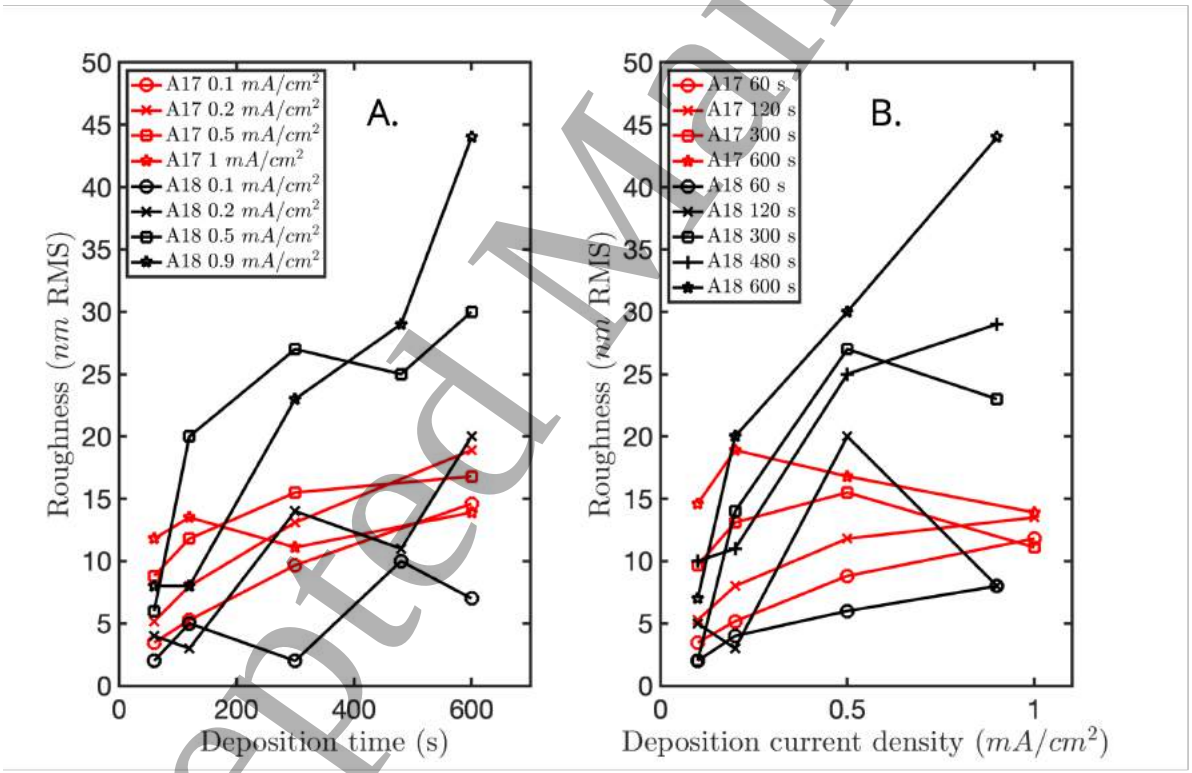


**Figure 9.** A. Roughness versus deposition time at constant deposition current densities. B. Roughness versus deposition current density at constant deposition times. A17 = Antensteiner and Abidian (2017), A18 = Antensteiner (2018).

### *3.3.3. Coating structure*

The influence of deposition materials and methods including deposition mode and co-ion on coating morphology was studied systematically in eight papers (Cui and Martin; 2003; Green et al.; 2011, 2012; Zhou et al.; 2013; Baek et al.; 2014a; Castagnola

et al.; 2014; Gunapu and Vanjari; 2017; Bodart et al.; 2019). The deposition mode (PS, GS, CV or GD) achieves different outcomes regardless of other deposition method choices. PS deposition results in individual grain-like structure from 2 $\mu m$ to 5 $\mu m$, while GS deposition yields a wavy but continuous structure (figure 6 A. and B.) (Cui and Martin; 2003). Microscopically, PS and GS show a similar cauliflower-like structure with PEDOT-rich grains separated by low concentration areas (PSS-rich areas), while CV deposition yields a more uniform coating (Castagnola et al.; 2014). CV deposition results in lower roughness coatings with higher intrinsic conductivity where charges travel more easily between the connected grains (Castagnola et al.; 2014). PS and GS grain structures have the opposite effect, reducing conductivity slightly but increasing roughness. For both PS and GS depositions, the number of PEDOT:PSS nuclei and the grain size increase with deposition time and with applied potential/current.

Zhou et al. (2013) compared PS and GS depositions of PEDOT:MWCNT with GS-deposited PEDOT:PSS (figure 6 F. - K.). For PEDOT:MWCNT, PS deposition yielded a wide and flat coating, overflowing to twice the substrate electrode diameter (100 $\mu m$), while GS deposition grew in a cone shape of smaller diameter than the substrate with greater roughness, and the PEDOT:PSS coating grew in a cylindrical shape, comparable to the GS-deposited PEDOT:MWCNT (figure 6, respectively J. and H.). Structurally, PS coatings formed compact globular particles while GS coatings formed a porous tangled rod structure and PEDOT:PSS exhibited the well-known cauliflower structure. When functionalized MWCNTs are added to PEDOT:PSS, a rougher, more porous structure is obtained (Gunapu and Vanjari; 2017). PSS co-ion creates smoother coatings compared with pTS and $ClO_4$ co-ions (figure 6 C. - E.) (Green et al.; 2012; Baek et al.; 2014a). Coating structures with pTS and $ClO_4$ co-ions are different, and vary between studies: pTS exhibited larger, bulkier grains than $ClO_4$ coatings in Green et al. (2011, 2012), and smaller grains than $ClO_4$ in Baek et al. (2014a).

Solvent choice also influences coating morphology: deionised water results in compact, rough, homogenous depositions, while organic solvents (acetonitrile and propylene carbonate) create porous coatings, which are less homogenous for the latter and prone to overgrowth (Bodart et al.; 2019). However, surface morphology was reported to be rougher with acetonitrile solvent, independent of co-ion choice in Poverenov et al. (2010). The differing conclusions may be due to the difference in electrode shape (conical for Bodart et al. (2019), flat for Poverenov et al. (2010)).

### *3.4. Electrode impedance*

Electrochemical Impedance Spectroscopy (EIS) measures the complex impedance response of an electrode to a small amplitude AC excitation. EIS is usually carried out at or near the OCP (table 8) and with a small excitation amplitude such that the electrode response remains linear (table 7). PEDOT coatings aim to reduce electrode impedance to reduce electrode noise and impedance imbalance and improve electrode performance for neural recording (Guo; 2020; Petrova; 1999; Mierzejewski et al.; 2020; Chung et al.;

2015; Boehler et al.; 2020; Ludwig et al.; 2011). We note that the measurement setup for EIS, with a small excitation amplitude, is not applicable to neural stimulation electrodes, and stimulation relevant measurements are presented in sections 3.1, 3.5, and 3.6.

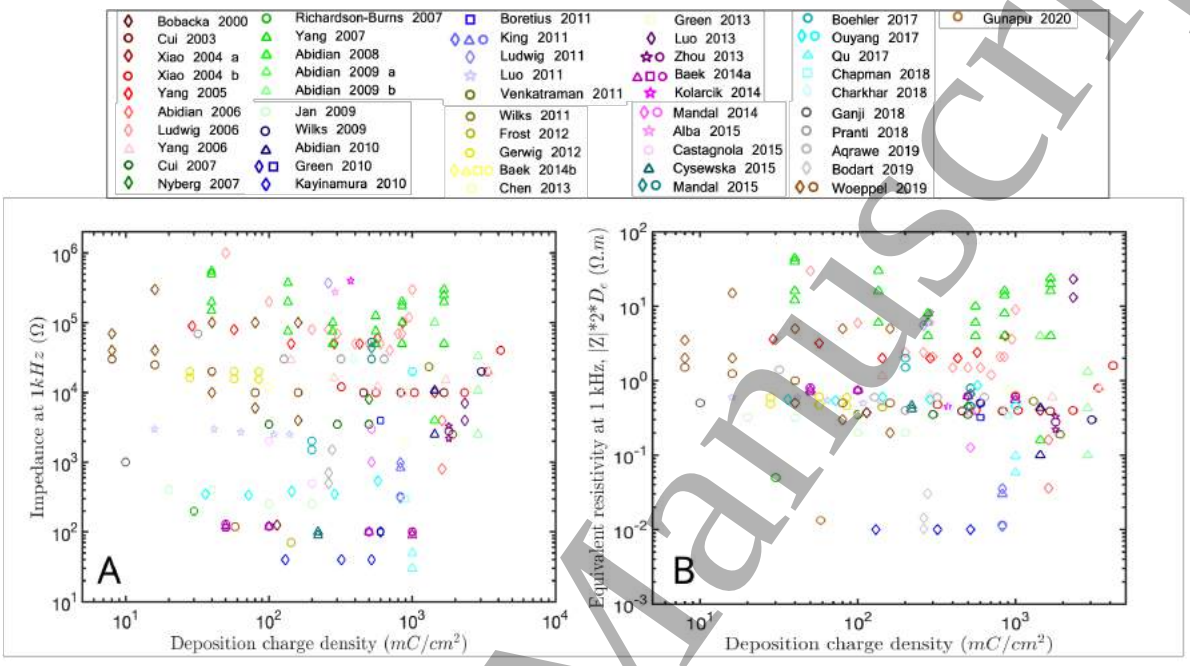


**Figure 10.** A. Electrode impedance at 1 kHz plotted against deposition charge density. Co-ions are indicated by marker shape: ○ for PSS, Δ for $ClO_4$, □ for pTS, ⋆ for MWCNT and ◊ for other species. B. Equivalent resistivity at 1 kHz plotted against deposition charge density normalised using equation 2.

Figure 10 A. shows the relationship between electrode impedance and deposition charge density. No clear trend in impedance magnitude with deposition is observed, although all PEDOT coated electrode impedances are expected to be lower compared with uncoated electrodes (Ludwig et al.; 2011). Observed impedance depends upon electrode geometry: when normalised to an equivalent 1 kHz resistivity using electrode geometry according to equation 2 (Newman; 1966), the majority of coatings have an equivalent resistivity of approximately 50 $\Omega.cm$ (PBS $\approx$ 72 $\Omega.cm$ (Chung et al.; 2015), figure 10 B.). Lower equivalent resistivities are observed for highly non-planar electrode geometries (Kayinamura et al.; 2010; Bodart et al.; 2019) and PEDOT/$MoS_2$ composite coatings (Gunapu et al.; 2020). To better understand trends in electrode impedance, reports with 5 or more different charge densities were considered (figure 11). For large electrode impedances ($> 1\ k\Omega$), and below a threshold charge density (between $10^2\ mC/cm^2$ and $10^3\ mC/cm^2$), impedance is negatively correlated with deposition charge density: increasing charge density reduces electrode impedance. However; above a threshold of PEDOT deposition charge density (e.g. $>700\ mC/cm^2$ in Ludwig et al. (2006)) electrode impedance is positively correlated with deposition charge, attributed to coating delamination (Ludwig et al.; 2006) and reductions in coating roughness (Yang

et al.; 2007, 2005; Xiao, Cui, Hancock, Bouguettaya, Reynolds and Martin; 2004; Xiao, Cui and Martin; 2004; Yang and Martin; 2006).

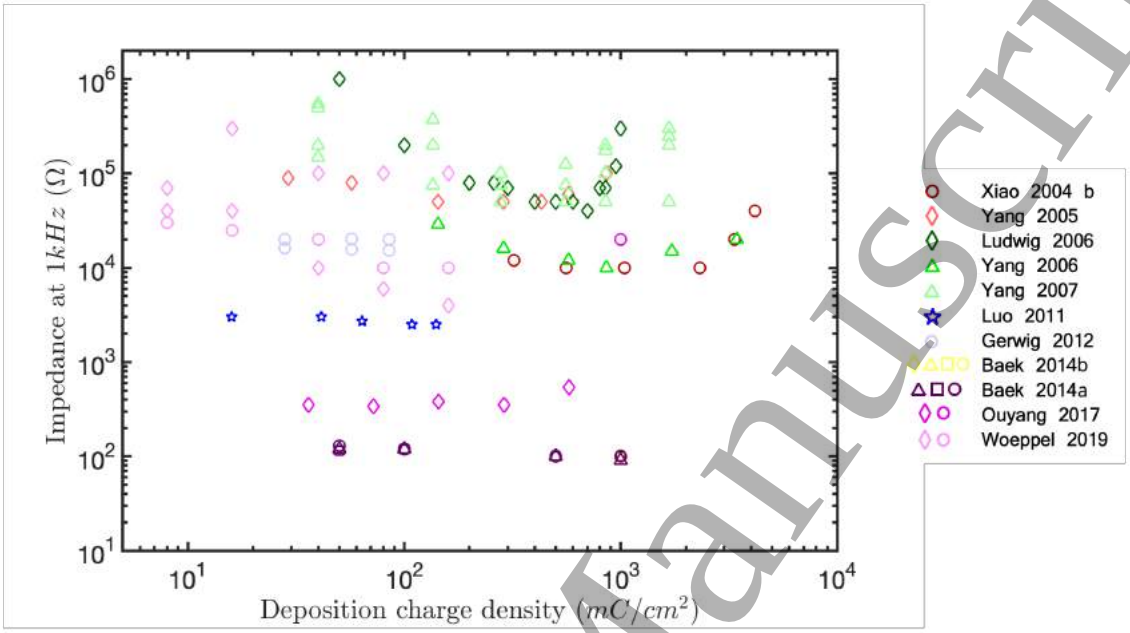


**Figure 11.** Electrode impedance at 1 kHz plotted against deposition charge density for studies with at least or more different charge densities. Co-ions are indicated by marker shape: ○ for PSS, Δ for $ClO_4$, □ for pTS, ⋆ for MWCNT and ◊ for other species. Baek 2014a overlaps Baek 2014b and is therefore not visible on the graph.

### *3.5. Charge storage capacity*

PEDOT coatings aim to increase CSC to improve electrode performance for neural stimulation.

Figure 12 shows the relationship between CSC and deposition charge density. CSC increases linearly with deposition charge density, despite the difference in other deposition materials and methods and CV parameters. Clear positive correlations are reported in some studies (Yang et al.; 2005; Luo et al.; 2011; Antensteiner and Abidian; 2017), while a few studies report different trends. Bodart et al. (2019) shows high CSC, which could be explained by the use of acetonitrile and PC as solvent, yielding porous and rough coatings with overgrowth, see section 3.3. Ouyang et al. (2017) report constant CSC of 2 $mC/cm^2$ to 2.5 $mC/cm^2$ for deposition charge densities between 30 $mC/cm^2$ and 600 $mC/cm^2$ on ITO and increased CSC to 7.85 $mC/cm^2$ on Pt for 1000 $mC/cm^2$ deposition charge density. The constant values are reported for a functionalized PEDOT-$NH_2$ to be used as adhesion layer, while the higher CSC corresponds to PEDOT:PSS. PEDOT-$NH_2$ does not form a polymer matrix like other co-ions, thus the coating does not grow with higher deposition charge densities and the CSC does not change (Ouyang et al.; 2017). Co-ion choice also influences CSC:

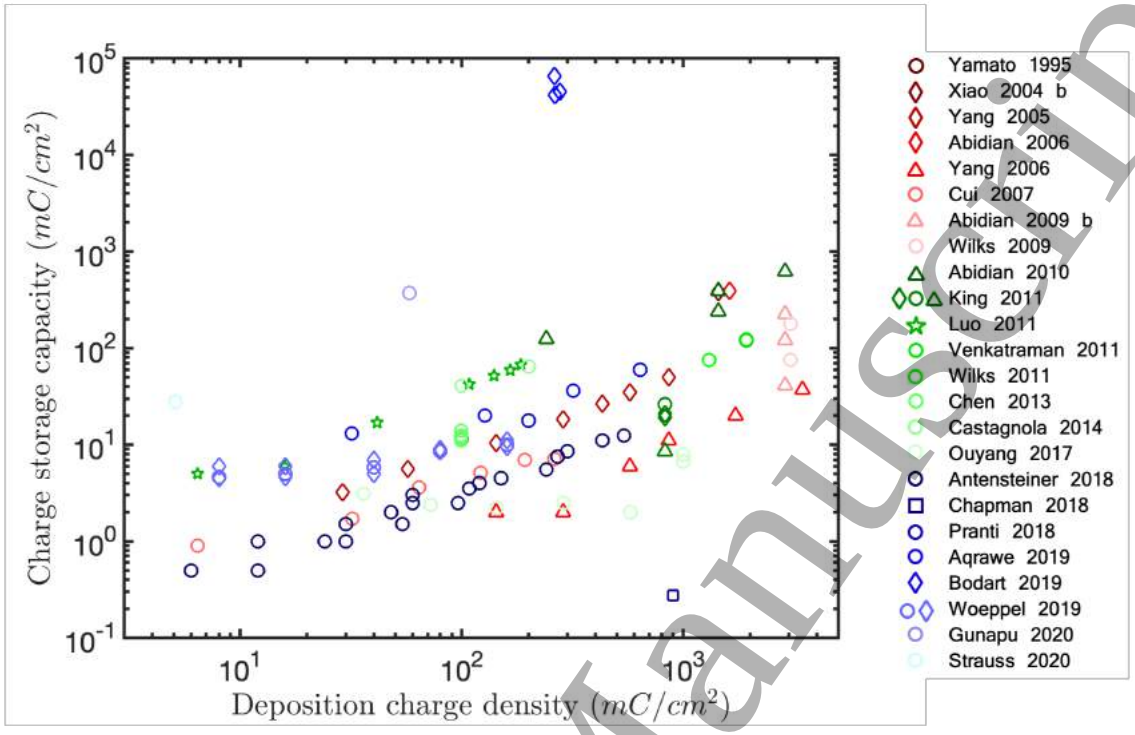


**Figure 12.** Charge storage capacity versus deposition charge density. Co-ions are indicated by marker shape: ○ for PSS, Δ for $ClO_4$, □ for pTS, ⋆ for MWCNT and ◊ for other species. "Castagnola 2014" refers to Castagnola, Maiolo, Maggiolini, Minotti, Marrani, Maita, Pecora, Angotzi, Ansaldo, Boffini, Fadiga, Fortunato and Ricci (2015).

porous, rough and thick coatings yield larger CSC because of their larger real surface area. King et al. (2011) report comparable CSC for heparin (20.9 $mC/cm^2$), $Cl^-$ (19.3 $mC/cm^2$) and PSS (26.1 $mC/cm^2$) co-ions and a lower CSC for $ClO_4$ (8.9 $mC/cm^2$) co-ion. This result is counter intuitive, as $ClO_4$ increases coating roughness, which should increase the surface area and therefore increase CSC. Alba et al. (2015) reported that PEDOT:MWCNT had a 5 times higher CSC than uncoated sites which decreased over time in vivo. Abidian and Martin (2009) demonstrate that for the same deposition methods, the addition of PEDOT nanotubes and hydrogel increases CSC.

Observed CSC is sweep rate dependent. At identical deposition charge density, fast sweep rate (1 V/s) yielded a 2.4 times larger CSC than slow sweep rate (50 mV/s), with a wide square-shaped voltammogram compared to well-defined peaks on the slow sweep rate voltammogram (Wilks et al.; 2009).

### *3.6. Charge injection limit*

Charge injection limit (CIL) is the maximum injectable charge during a current pulse before the electrode potential reaches the onset of harmful reactions, usually the water window. CIL is measured using CP, sending biphasic current pulses of increasing

intensity and recording the electrode potential. Test parameters including pulse width and test solution can have a considerable influence on observed CIL. Several pulse widths were used across studies, so we considered the influence of pulse width on observed CIL (Figure 13). To compare between studies the influence of deposition charge density on CIL was examined for the two most used pulse widths (figure 14). PEDOT coatings aim to increase CIL to improve electrode performance for neural stimulation.

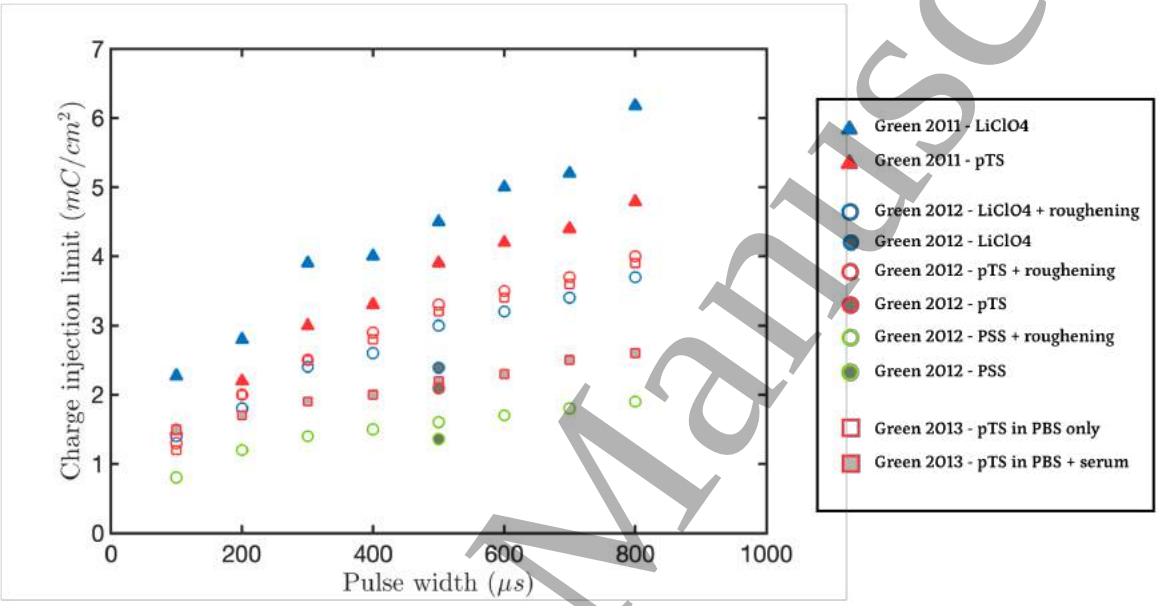


**Figure 13.** Charge storage capacity versus pulse width for identical deposition charge density. Filled markers indicate anodic-first stimulation and empty markers indicate cathodic-first stimulation.

Three studies reported the effect of pulse width on CIL, keeping the same deposition strategy (Green et al.; 2010, 2012, 2013). All studies showed an increase in the CIL with pulse width. Anodic-first pulses resulted in higher CIL than cathodic-first pulses. Green et al. (2011) report higher CIL for $ClO_4$ than pTS co-ions, while Green et al. (2012) shows that pTS co-ions generate a slightly higher CIL, and that both $ClO_4$ and pTS co-ions exhibit larger CIL than PSS co-ions. Laser roughening of the substrate before coating increases CIL for all co-ions, and the influence was greater for pTS and $ClO_4$ than for PSS co-ions (Green et al.; 2012). The CIL of pTS co-ion coatings is lower than $ClO_4$ without roughening. Green et al. (2013) show that observed the CIL decreases when serum is added to a PBS test solution.

For 200 $\mu$s pulse width, the CIL increases with deposition charge density (figure 14 A.). Zhou et al. (2013) shows increased CIL when adding MWCNT to PEDOT, especially for anodic-first pulses, which exhibit a higher CIL than cathodic-first. The discrepancy in Green et al. (2011) and Green et al. (2012) for identical deposition charge densities is due to different co-ion, while Green et al. (2013) report lower CIL when adding serum to PBS.

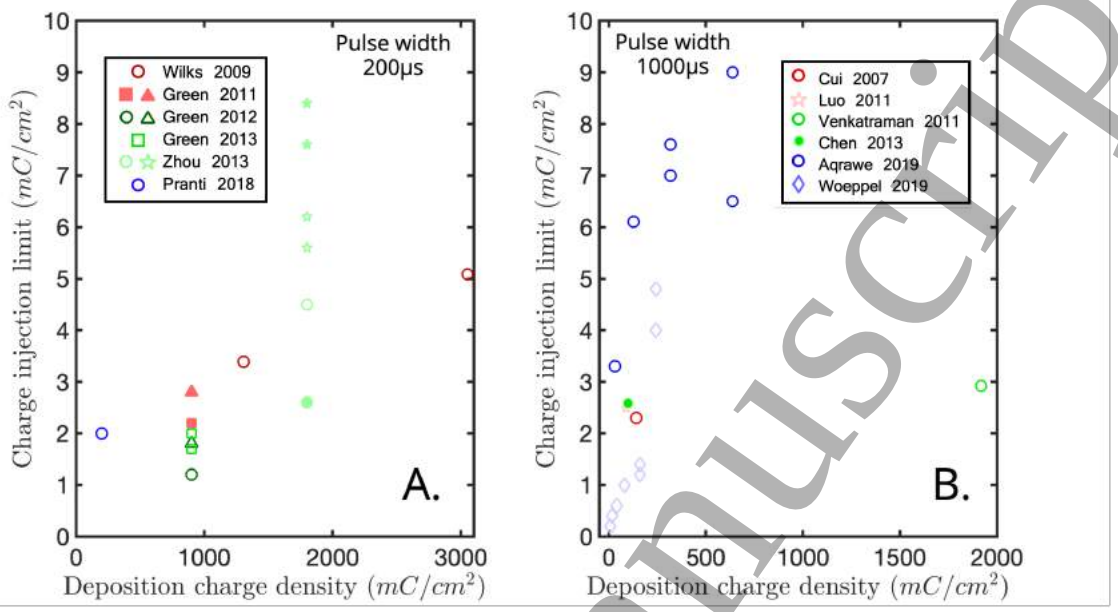


**Figure 14.** A. Charge injection limit versus deposition charge density for 200 $\mu$s pulse width. B. Charge injection limit versus deposition charge density for 1000 $\mu$s pulse width. Filled symbols represent anodic-first pulses. Co-ions are indicated by marker shape: ○ for PSS, Δ for $ClO_4$, □ for pTS, ⋆ for MWCNT and ◊ for other species. Filled markers indicate anodic-first stimulation and empty markers indicate cathodic-first stimulation.

For 1000 $\mu$s pulse width, the CIL also increases with deposition charge density, with a steeper slope than at 200 $\mu$s (figure 14 B.). Venkatraman et al. (2011) observed a relatively low CIL for a 1920 $mC/cm^2$ deposition charge density, which could be explained by a different electrode shape: a wire tip concentrates the electric field, causing larger potential gradients than for disc electrodes.

## 4. Discussion

Despite the wide range of PEDOT coating electrodeposition methods and characterisation methods reported, clear correlations have been observed. Deposition charge density is positively correlated with coating thickness, coating roughness, charge storage capacity, and charge injection limit. Electrode impedance shows dependence on electrode radius rather than charge density for the majority of studies outside extremes of deposition charge density. Other method choices including deposition mode and solvent have important effects on coating morphology and structure, which affect electrode performance.

***PEDOT coating methods*** Substrate, co-ion, and deposition mode choice are dominated by a few common choices: gold or platinum; PSS, $ClO_4$, or pTS; and GS,

PS, or CV respectively. A few trends are attributed to reproducing research protocols within the same research group, including using 0.05 M pTS as co-ion; however, most effects seem to be independent of the research group. Naturally, protocols tend to be reproduced from previous successful studies, as for instance the four earliest studies considered in this review used the same EDOT and co-ion concentrations (Yamato et al.; 1995; Bobacka; 1999; Bobacka et al.; 2000; Cui and Martin; 2003).

Co-ion concentrations and EDOT concentrations varied by as much as 1 order of magnitude between studies. Higher co-ion concentrations may inhibit monomer oxidation at the electrode surface and may trap charges in the coating structure, increasing impedance (Kayinamura et al.; 2010). However, this effect was not confirmed in this review when considering only the 1 kHz impedance. The impedance increase may apply to other frequency ranges, and other factors such as electrode size and shape dominate the implant's impedance.

***PEDOT characterisation methods*** Choices of characterisation method and parameters, for example not conducting EIS at OCP, may influence the reported results. However, we find here that reported 1 kHz impedances were not substantially different for EIS at OCP than at other potentials. Differences may arise at low frequencies, but these values were not consistently reported (Boehler et al.; 2020).

Choosing the sweep rate for CV as a compromise may result in losing the benefits of both slow and fast CV. To have a detailed representation of possible reactions and calculate an accurate CSC, a slower sweep rate is needed (10 mV/s or slower). However, slow CV does not allow accurate representation of the possible reactions during a pulse, since slow CV depicts a quasi-equilibrium state, whereas during a short stimulation pulse, the potential change rate is of the order of 100 V/s, far from equilibrium conditions.

CP should be conducted at the pulse width that is to be used in vivo. Therefore, pulse widths greater than 200 $\mu s$ may not represent the true CIL of electrodes intended for use for neural stimulation with typical pulse widths in vivo of 100 $\mu s$ or 200 $\mu s$.

***Coating morphology*** PEDOT coating morphology, including thickness and roughness, depends upon deposition charge density. High current density does not guarantee a rough coating: to achieve an increase in roughness a long deposition time may be required (figure 9). For low current densities (0.1 $mA/cm^2$ to 0.5 $mA/cm^2$) a regular increase of roughness with time occurs but low overall roughness is achieved, even for long depositions. At medium current density (0.5 $mA/cm^2$), large roughnesses may be achieved with limited deposition time, with maximum in roughness depending on charge density (Antensteiner and Abidian (2017) shows limited roughness for the highest charge densities and longest time). The plateau observed by Antensteiner and Abidian (2017), which was not present in Antensteiner (2018), can be explained by the change of EDOT:PSS ratio: by using a 10 times larger PSS concentration, Antensteiner (2018) may have allowed more PSS to deposit to create PEDOT grains, increasing roughness,

while Antensteiner and Abidian (2017) may have exhausted the PSS. This hypothesis is supported by Yang and Martin (2006), which used the same ratio as Antensteiner and Abidian (2017) and observed a similar plateau of roughness.

The consistency in this result between studies demonstrates that deposition charge density determines PEDOT coating thickness. Variation in thickness between individual studies can be explained by variation in other deposition factors, such as addition of MWCNT or use of specific solvents to template the coating. Besides MWCNT, co-ion choice did not influence PEDOT coating thickness significantly.

***Electrode impedance*** Impedance at 1 kHz was the most consistently reported result for EIS measurement; however, 1 kHz EIS is insufficient to fully describe the electrode behaviour (Boehler et al.; 2020). 1 kHz impedance is negatively correlated with deposition charge density under some conditions, also depending on electrode geometry, test conditions, and coating stability and roughness.

PEDOT coatings increase electrode capacitance, such that for the majority of reporting studies the capacitive reactance at 1 kHz is lower than the spreading resistance of the solution ($R_s$). Therefore, electrode geometry and solution resistivity prevail in the observed impedance, the 1 kHz response is near ohmic, and scales roughly inversely with radius ($r^{-1}$) according to equation 2 (Chung et al.; 2015; Kayinamura et al.; 2010; Newman; 1966; Fan et al.; 2021; Ganji et al.; 2017; Wang, Jung, Lee and Wang; 2021; Proctor et al.; 2016), shown in the consistent equivalent resistivity values between studies (figure 10 B.). Increasing deposition charge density increases capacitance without reducing electrode impedance unless the coating changes the electrode geometry or roughness (Ouyang et al.; 2017; Baek et al.; 2014a; Luo et al.; 2011; Gerwig et al.; 2012; Yang and Martin; 2006). We hypothesise that PEDOT coated electrode 1 kHz impedance will scale roughly with area ($r^{-2}$) only for low deposition charge densities, where coating volume and therefore double layer capacitance is not substantially increased, or small electrodes, where capacitance governs the observed impedance (Ganji et al.; 2017; Wang, Jung, Lee and Wang; 2021; Proctor et al.; 2016). The transition from radial to areal 1 kHz impedance scaling has been observed below radius $\approx 100\ \mu m$ for both Au and Pt PEDOT:PSS spin coated electrodes, compared with radius $\approx 1000\ \mu m$ for uncoated Au and Pt electrodes (Ganji et al.; 2017; Wang, Jung, Lee and Wang; 2021). An additional transition from areal to radial scaling is observed below 10 $\mu m$ radius for Pt electrodes, a transition which has not been reported with PEDOT coatings (Fan et al.; 2021).

No clear influence of co-ion on EIS was observed. $ClO_4$ seemingly correlated with higher 1 kHz impedance, however studies testing different co-ions reported similar EIS values (Baek et al.; 2014a,b). Therefore, we hypothesize that the higher 1 kHz impedance for $ClO_4$ was due to other materials or methods. Among the papers reporting high 1 kHz impedance with $ClO_4$, a series by Abidian (2008; 2009; 2009; 2010) used a PLLA template to form PEDOT nanotubes, which increased coating thickness and CSC, but possibly also increased 1 kHz impedance. We can notice however, that in the two

latest studies (Abidian and Martin; 2009; Abidian et al.; 2010), the normalised 1 kHz impedance fell in line with other studies and even below. Another study standing out is from Yang et al. (2007), which used polyacrylic acid (PAA) to form PEDOT nanofibrils could offer a similar explanation. Besides, normalised 1 kHz impedances in other studies using $ClO_4$ mostly follow the same trend as other co-ions.

For some studies, above a threshold, impedance is positively correlated with deposition charge density. Negative correlations between impedance and deposition charge density are attributable to increased electrode capacitance and area. Positive correlations at high deposition charge densities have been attributed to delamination of thick coatings during handling (Ludwig et al.; 2006), and reductions in coating roughness and porosity at charge densities above $8 \times 10^2$ $mC/cm^2$ (Yang et al.; 2007), $1 \times 10^3$ $mC/cm^2$ (Yang et al.; 2005), or $1.5 \times 10^3$ $mC/cm^2$ (Xiao, Cui, Hancock, Bouguettaya, Reynolds and Martin; 2004; Xiao, Cui and Martin; 2004; Yang and Martin; 2006) (a series of studies from a single laboratory).

***Charge storage capacity*** CSC is strongly correlated with deposition charge density (figure 12). PEDOT coating is inherently rough and porous, significantly increasing real electrode surface area and therefore CSC. Increasing coating thickness and roughness with increased deposition charge density explain increases in CSC. In contrast to Pt CSC by pseudocapacity of 294 $\mu C/cm^2$ (Merrill et al.; 2005), and Pt CSC observations ranging from 150 $\mu C/cm^2$ to 5.6 $mC/cm^2$ depending upon CV parameters (Harris et al.; 2018), CSC can be increased by PEDOT coating: 4.3× (Strauss et al.; 2020); 8.6× (Ouyang et al.; 2017); and 15× (Venkatraman et al.; 2011) in example studies. Deposition materials or methods which change PEDOT coating morphology also affect the CSC, such as acetonitrile solvent which increases roughness, real electrode area, and thus increases CSC (Bodart et al.; 2019). Co-ion choice, and co-deposited coatings, can tailor CSC, reducing CSC with $ClO_4$ co-ions (King et al.; 2011), or increasing with MWCNT co-coatings (Alba et al.; 2015).

PEDOT:PSS coating capacitance is proportional to deposited PEDOT volume (Bianchi et al.; 2022; Proctor et al.; 2016). In this review we show a positive correlation between CSC and deposition charge density (figure 12), and a positive correlation between thickness and deposition charge density (figure 7); therefore there is a correlation between CSC and deposited PEDOT volume.

***Charge injection limit*** CIL was highly influenced by co-ion choice and correlated positively with pulse width and deposition charge density. The testing solution played an important role in CIL measurement as the addition of serum notably decreased the CIL, partially explaining differences between in vitro and in vivo results.

Many observed differences are due to substrate or characterisation choices, rather than PEDOT coating methods. CIL increases with substrate laser roughening (Green et al.; 2012), attributable to increased real surface area. CIL decreases when serum is added (Green et al.; 2013) due to proteins adsorbing onto the electrode surface, reducing

the charge-transfer area and increasing polarisation.

***Topics not covered*** This review aimed to summarise the methods used for PEDOT electrodeposition on metallic electrodes to be able to compare deposition routes.

The variety of parameters of characterisation methods makes interpretation and comparison challenging without apparent justification. With new methods developing, such as PEDOT hydrogels and in situ polymerization, it is crucial that methods are reported extensively and as uniformly as possible, so performances can be compared and reproduced.

This review has not investigated long-term stability of PEDOT coatings, or their performance in vivo for recording and stimulation. The wide range of analysis methods for stability and in vivo performance make direct comparisons and synthesis of results challenging. Nevertheless efficient recording capability and long-term stability are key challenges of the use of PEDOT coatings. PEDOT may crack and delaminate under electrochemical stress or delaminate with handling (Ludwig et al.; 2006; Cui and Zhou; 2007; Jan et al.; 2009; Boehler et al.; 2017). Adverse body response is reduced for PEDOT coated electrodes compared with bare metal; however, body response still affects neural implants' long term performance and stability of PEDOT coatings in chronic experiments (Ludwig et al.; 2006). Common co-ions including MWCNTs and NPs acted to form PEDOT nanocomposites, which are favored for next generation implants; however, key mechanical and biological advantages of nanocomposites including coating stability and neuron response were not addressed in this review (Adekoya et al.; 2021; Depan and Misra; 2014). Substrate adhesion and mitigation of body response are key lines of investigation for PEDOT coatings to prolong neural electrode efficacy.

## Conclusion

The wide range of materials and methods used for PEDOT deposition illustrates its versatility and "tunability". The impact of deposition methods on specific performances (EIS, CV, CP) and correlations between morphology and performance were highlighted. Electrode performance and integration represents a broader challenge, and where thickness and roughness need to be increased to reduce impedance and increase CSC, it may compromise mechanical stability, as thick coatings are more likely to crack and delaminate (Cui and Martin; 2003). PEDOT coating performance is highly dependent upon coating materials and methods. Trade-offs exist between different outcomes and performances, for example coating thickness, CSC, and stability. This review cannot recommend a best, or one-size-fits-all method for PEDOT electrodeposition. In particular, differences between characterisation methods and reported values make robust comparisons challenging, and we encourage researchers to report their methods fully and reproducibly and to share their experimental data.

## Appendix

### *4.1. Characterisation method parameters*

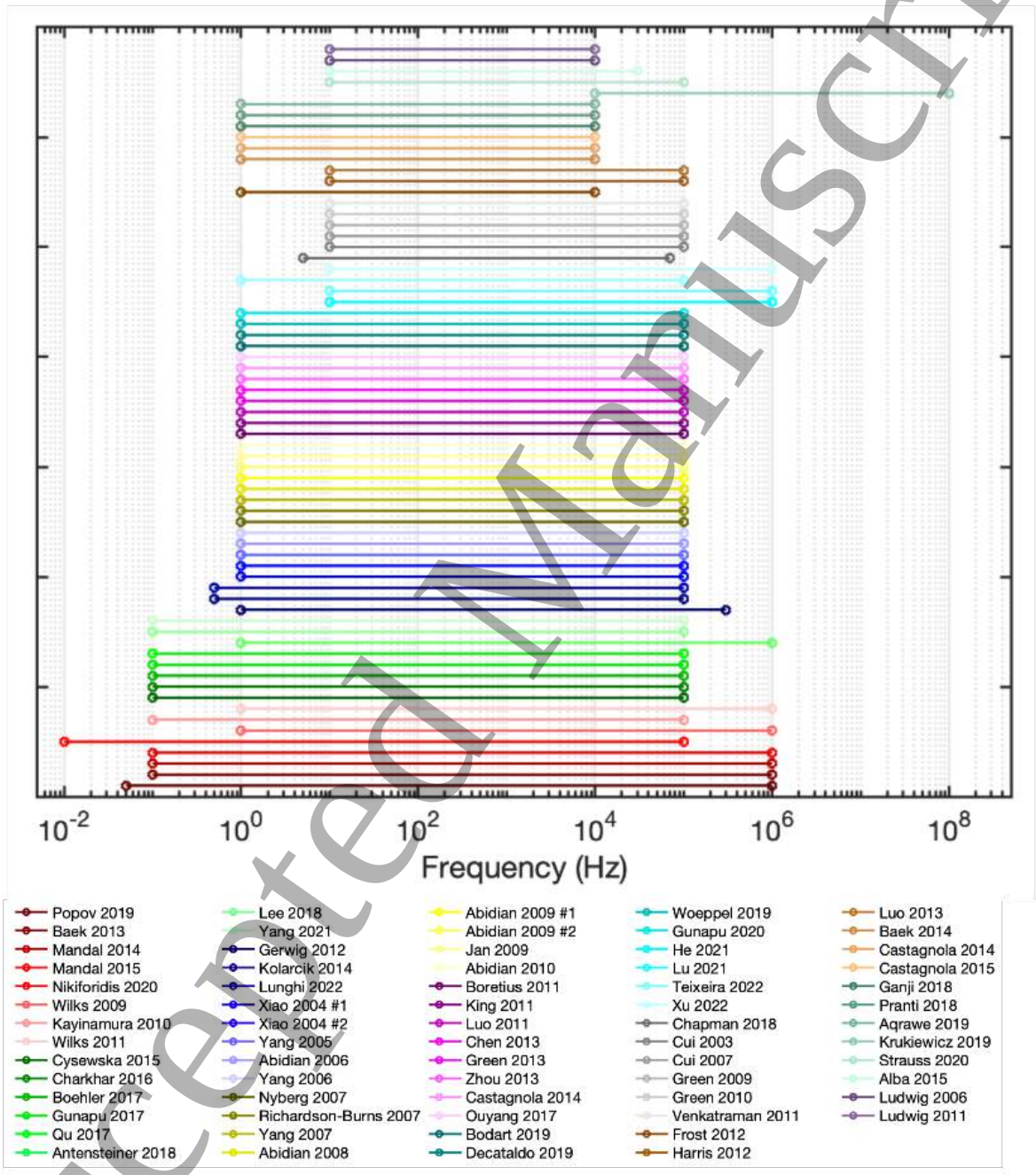


**Figure 15.** Reported frequency ranges for electrochemical impedance spectroscopy (EIS) of PEDOT coated neural interfaces. The frequency ranges are plotted from the widest to the narrowest.

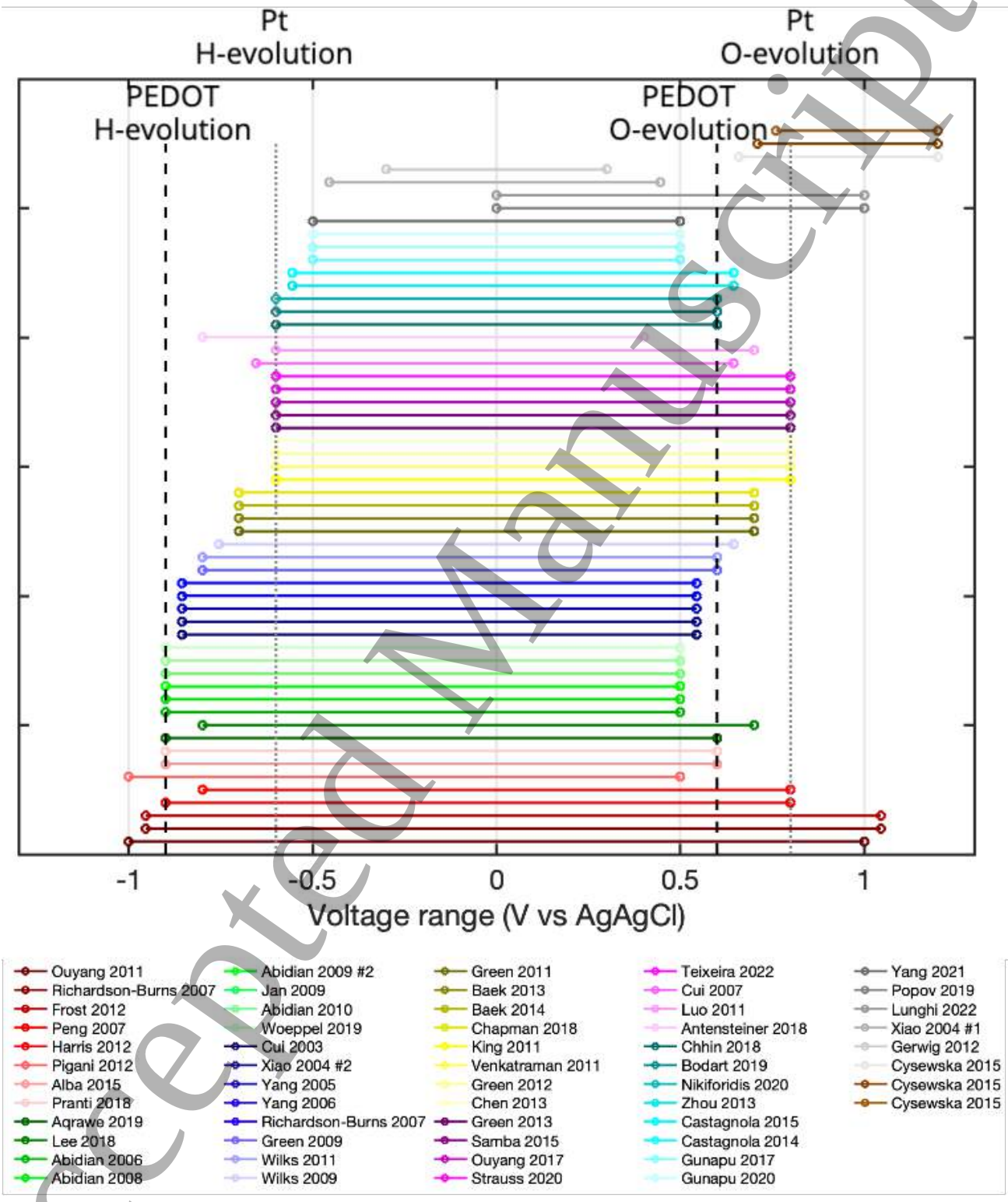


**Figure 16.** Reported voltage ranges for cyclic voltammetry (CV) of PEDOT coated neural interfaces. The water window is indicated respectively by black intermittent lines for PEDOT coated electrodes and grey dotted lines for Pt and PtIr substrates (Cogan et al.; 2016).

q

**Table 2.** Number of studies reporting each PEDOT coating substrate.

| **Substrate** | **Au**[1] | **Pt**[2] | **PtIr**[3] | **Ir**[4] | **SS**[5] | **Au NPs**[6] | **ITO**[7] | **Mg**[8] | **Others**[*] |
|---|---|---|---|---|---|---|---|---|---|
| **Study count** | 39 | 20 | 8 | 5 | 4 | 3 | 3 | 2 | 7 |

*Others included iridium oxide (Boehler et al.; 2017), glassy carbon (Bobacka; 1999), gold nanorods (Ganji et al.; 2018), graphite (Cysewska et al.; 2015), platinum nanograss (Boehler et al.; 2017), platinum nanoparticles (Lu et al.; 2021) and fluorine-doped tin oxide ($SnO_2 - F$)(Bhandari et al.; 2009).

[1] Gold, Cui and Martin (2003); Xiao, Cui, Hancock, Bouguettaya, Reynolds and Martin (2004); Xiao, Cui and Martin (2004); Yang et al. (2005); Abidian et al. (2006); Yang and Martin (2006); Abidian et al. (2007); Richardson-Burns et al. (2007); Yang et al. (2007); Abidian and Martin (2008); Abidian et al. (2009); Abidian and Martin (2009); Jan et al. (2009); Abidian et al. (2010); Kayinamura et al. (2010); Ludwig et al. (2011); Gerwig et al. (2012); Chen et al. (2013); Luo et al. (2013); Castagnola et al. (2014); Castagnola, Maiolo, Maggiolini, Minotti, Marrani, Maita, Pecora, Angotzi, Ansaldo, Boffini, Fadiga, Fortunato and Ricci (2015); Mandal et al. (2014); Castagnola, Descamps, Lecestre, Dahan, Remaud, Nowak and Bergaud (2015); Kozai et al. (2015); Mandal et al. (2015); Samba et al. (2015); Charkhkar et al. (2016); Antensteiner and Abidian (2017); Gunapu and Vanjari (2017); Antensteiner (2018); Ganji et al. (2018); Pranti et al. (2018); Aqrawe et al. (2019); Decataldo et al. (2019); Woeppel et al. (2019); Gunapu et al. (2020); Nikiforidis et al. (2020); He et al. (2021); Yang et al. (2021); Teixeira et al. (2022)

[2] Platinum, Yamato et al. (1995); Bobacka et al. (2000); Cui and Zhou (2007); Peng et al. (2007); Green et al. (2009, 2010); Boretius et al. (2011); Green et al. (2011); Luo et al. (2011); Green et al. (2011); Pigani et al. (2012); Baek et al. (2014b); Green et al. (2013); Zhou et al. (2013); Baek et al. (2014a); Boehler et al. (2017); Ouyang et al. (2017); Chhin et al. (2018); Krukiewicz et al. (2019); Xu et al. (2022)

[3] Platinum/Iridium Alloy, Jan et al. (2009); King et al. (2011); Venkatraman et al. (2011); Luo et al. (2013); Kolarcik et al. (2014); Alba et al. (2015); Bodart et al. (2019); Strauss et al. (2020)

[4] Iridium, Ludwig et al. (2006); Wilks et al. (2009); Wilks (2011); Harris et al. (2012); Ouyang et al. (2017)

[5] Stainless Steel, Ouyang et al. (2011); Frost et al. (2012); Qu (2017); Chapman et al. (2018)

[6] Gold Nanoparticles, Lee et al. (2018); Krukiewicz et al. (2019); Lunghi et al. (2022)

[7] Indium tin oxide, Nyberg et al. (2007); Ouyang et al. (2017); Popov et al. (2019)

[8] Magnesium, Sebaa et al. (2013); Zhang et al. (2018)

**Table 3.** Number of studies reporting each PEDOT co-ion.

| Co-ion | PSS[1] | $ClO_4$[2] | pTS[3] | MWCNT[4] | $BF_4$[5] | DCDPG-YIGSR[6] | TEAP[7] |
|---|---|---|---|---|---|---|---|
| Study count | 46 | 20 | 13 | 6 | 3 | 3 | 3 |

| Co-ion | PBS[8] | KCl[9] | NaCl[10] | DEDEDY-FQRYLI[11] | [EMIM] [Tf2M][12] | Dex[13] | Others* |
|---|---|---|---|---|---|---|---|
| Study count | 5 | 2 | 2 | 2 | 2 | 2 | 24 |

*Others included: peptide CDPGYIGSR (Xiao, Cui, Hancock, Bouguettaya, Reynolds and Martin; 2004), sulfonatoalkoxy EDOT (S-EDOT) (Xiao, Cui and Martin; 2004), PEDOT:PSS (Nyberg et al.; 2007), carbon nanotubes (CNT) (Peng et al.; 2007), lithium triflate ($LiCF_3SO_3$) (Bhandari et al.; 2009), hexafluorophosphate ($PF_6$) (Kayinamura et al.; 2010), dihydrogenphosphate ($H_2PO_4$) (King et al.; 2011), tetrabutylammonium perchlorate (TBAP) (King et al.; 2011), heparin (King et al.; 2011), glutamate (King et al.; 2011), human albumin (King et al.; 2011), bovine serum albumin (King et al.; 2011), poly(d-lysine) (King et al.; 2011), biotin (King et al.; 2011), sulfate ($SO_4$) (Harris et al.; 2012), benzenesulfonate (Baek et al.; 2014b), dodecylbenzenesulfonate (Baek et al.; 2014b), graphene oxide (Luo et al.; 2013), azanide anion ($NH_2$) (Ouyang et al.; 2017), perchlorate and sulfuric acid ($ClO_4 + H_2SO_4$) (Popov et al.; 2019), aniline (Popov et al.; 2019), silica nanoparticles (Woeppel et al.; 2019) and no co-ion (Abidian et al.; 2006).

[1] Poly(sodium 4-styrenesulfonate), Yamato et al. (1995); Bobacka (1999); Bobacka et al. (2000); Cui and Martin (2003); Xiao, Cui, Hancock, Bouguettaya, Reynolds and Martin (2004); Cui and Zhou (2007); Richardson-Burns et al. (2007); Jan et al. (2009); Wilks et al. (2009); Kayinamura et al. (2010); King et al. (2011); Venkatraman et al. (2011); Wilks (2011); Frost et al. (2012); Gerwig et al. (2012); Green et al. (2012); Baek et al. (2014b); Chen et al. (2013); Luo et al. (2013); Zhou et al. (2013); Baek et al. (2014a); Castagnola et al. (2014); Castagnola, Maiolo, Maggiolini, Minotti, Marrani, Maita, Pecora, Angotzi, Ansaldo, Boffini, Fadiga, Fortunato and Ricci (2015); Mandal et al. (2014); Castagnola, Descamps, Lecestre, Dahan, Remaud, Nowak and Bergaud (2015); Kozai et al. (2015); Mandal et al. (2015); Samba et al. (2015); Antensteiner and Abidian (2017); Boehler et al. (2017); Gunapu and Vanjari (2017); Ouyang et al. (2017); Antensteiner (2018); Ganji et al. (2018); Pranti et al. (2018); Aqrawe et al. (2019); Decataldo et al. (2019); Woeppel et al. (2019); Gunapu et al. (2020); Nikiforidis et al. (2020); Strauss et al. (2020); He et al. (2021); Lu et al. (2021); Lunghi et al. (2022); Teixeira et al. (2022); Xu et al. (2022)

[2] Perchlorate ion, Yang and Martin (2006); Abidian et al. (2007); Peng et al. (2007); Yang et al. (2007); Abidian and Martin (2008); Abidian et al. (2009); Abidian and Martin (2009); Abidian et al. (2010); Kayinamura et al. (2010); Green et al. (2011); King et al. (2011); Green et al. (2012); Pigani et al. (2012); Baek et al. (2014b,a); Cysewska et al. (2015); Qu (2017); Chhin et al. (2018); Nikiforidis et al. (2020); Yang et al. (2021)

[3] p-Toluenesulfonate, Green et al. (2009, 2010); Kayinamura et al. (2010); Boretius et al. (2011); Green et al. (2011); King et al. (2011); Green et al. (2012); Harris et al. (2012); Baek et al. (2014b); Green et al. (2013); Baek et al. (2014a); Chapman et al. (2018)

[4] Multi-walled carbon nanotubes, Bhandari et al. (2009); Luo et al. (2011); Zhou et al. (2013); Kolarcik et al. (2014); Alba et al. (2015); Kozai et al. (2015)

[5] Tetrafluoroborate, Kayinamura et al. (2010); Mandal et al. (2014, 2015); Charkhkar et al. (2016); Bodart et al. (2019)

[6] Synthetic neuron-binding peptide DCDPGYIGSR, Cui and Martin (2003); Green et al. (2009, 2010)

[7] Tetraethylammonium perchlorate, Yang et al. (2005); Ludwig et al. (2006, 2011)

[8] Phosphate buffered saline solution, King et al. (2011); Ouyang et al. (2011); Krukiewicz et al. (2019)

[9] Potassium chloride, Bobacka (1999); Bobacka et al. (2000)

[10] Sodium chloride, Bobacka et al. (2000); King et al. (2011)

[11] Anionically modified laminin peptide DEDEDYFQRYLI, Green et al. (2009, 2010)

[12] 1-Ethyl-3-methylimidazolium bis(trifluromethylsulfonyl)imide, Sebaa et al. (2013); Zhang et al. (2018)

[13] Dextran, Lee et al. (2018); Krukiewicz et al. (2019)

**Table 4.** Number of studies and methods (entries) reporting each PEDOT deposition mode.

| **Deposition mode** | **GS**[1] | **PS**[2] | **CV**[3] | **GD**[4] |
|---|---|---|---|---|
| **Study count** | 50 | 28 | 14 | 2 |
| **Entry count**† | 383 | 108 | 45 | 15 |

† To account for studies comparing deposition modes we counted reported deposition method combinations (entries), for example a single study of GS deposition using two different co-ions would have study count 1, and entry count 2.

[1] Galvanostatic, Bobacka (1999); Bobacka et al. (2000); Cui and Martin (2003); Xiao, Cui, Hancock, Bouguettaya, Reynolds and Martin (2004); Xiao, Cui and Martin (2004); Yang et al. (2005); Abidian et al. (2006); Ludwig et al. (2006); Yang and Martin (2006); Abidian et al. (2007); Cui and Zhou (2007); Richardson-Burns et al. (2007); Yang et al. (2007); Abidian and Martin (2008); Abidian et al. (2009); Abidian and Martin (2009); Green et al. (2009); Jan et al. (2009); Wilks et al. (2009); Abidian et al. (2010); Green et al. (2010); Boretius et al. (2011); Green et al. (2011); King et al. (2011); Ludwig et al. (2011); Luo et al. (2011); Venkatraman et al. (2011); Wilks (2011); Frost et al. (2012); Green et al. (2012); Baek et al. (2014b); Chen et al. (2013); Green et al. (2013); Zhou et al. (2013); Baek et al. (2014a); Castagnola et al. (2014); Kolarcik et al. (2014); Cysewska et al. (2015); Kozai et al. (2015); Antensteiner and Abidian (2017); Ouyang et al. (2017); Qu (2017); Antensteiner (2018); Chapman et al. (2018); Pranti et al. (2018); Zhang et al. (2018); Bodart et al. (2019); Woeppel et al. (2019); Nikiforidis et al. (2020); Strauss et al. (2020)

[2] Potentiostatic, Yamato et al. (1995); Cui and Martin (2003); Peng et al. (2007); Nyberg et al. (2007); Bhandari et al. (2009); Kayinamura et al. (2010); Ouyang et al. (2011); Harris et al. (2012); Pigani et al. (2012); Luo et al. (2013); Sebaa et al. (2013); Zhou et al. (2013); Castagnola et al. (2014); Castagnola, Maiolo, Maggiolini, Minotti, Marrani, Maita, Pecora, Angotzi, Ansaldo, Boffini, Fadiga, Fortunato and Ricci (2015); Kolarcik et al. (2014); Mandal et al. (2014); Alba et al. (2015); Cysewska et al. (2015); Mandal et al. (2015); Antensteiner and Abidian (2017); Boehler et al. (2017); Gunapu and Vanjari (2017); Antensteiner (2018); Ganji et al. (2018); Aqrawe et al. (2019); Decataldo et al. (2019); Gunapu et al. (2020); Yang et al. (2021); Teixeira et al. (2022)

[3] Cyclic Voltammetry, Sebaa et al. (2013); Castagnola et al. (2014); Castagnola, Descamps, Lecestre, Dahan, Remaud, Nowak and Bergaud (2015); Charkhkar et al. (2016); Chhin et al. (2018); Lee et al. (2018); Zhang et al. (2018); Krukiewicz et al. (2019); Popov et al. (2019); He et al. (2021); Lu et al. (2021); Lunghi et al. (2022); Teixeira et al. (2022); Xu et al. (2022)

[4] Galvanodynamic, Gerwig et al. (2012); Samba et al. (2015)

**Table 5.** Number of studies reporting each PEDOT co-ion concentration for 4 major co-ions.

| [Co-ion] (M) | 0.01 | 0.02 | 0.03 mg/mL | 0.05 mg/mL | 0.06 | 0.07 | 0.08 | 0.1 | 0.11 | 0.13 | 0.2 |
|---|---|---|---|---|---|---|---|---|---|---|---|
| **PSS** | 1[1] | 10[2] | 3[3] | 4[4] | 1[5] | 2[6] | 2[7] | 18[8] | 2[9] | 1[10] | 1[11] |
| ***ClO*$_4$** | 2[13] | | | 3[14] | | | | 14[15] | | | |
| **pTS** | 1[17] | | | 8[18] | | | | 3[19] | | | |
| **MWCNT** | | | | | | | | | | | |

| [Co-ion] (M) | 0.29 | 0.5 | 1 | 2 | N/A |
|---|---|---|---|---|---|
| **PSS** | 1[12] | | | | 3 |
| ***ClO*$_4$** | | 1[16] | | | |
| **pTS** | | | | | |
| **MWCNT** | | | 3[20] | 2[21] | 1 |

- Poly(sodium 4-styrenesulfonate) (PSS) -

[1] King et al. (2011)

[2] Richardson-Burns et al. (2007); Jan et al. (2009); Venkatraman et al. (2011); Chen et al. (2013); Castagnola, Descamps, Lecestre, Dahan, Remaud, Nowak and Bergaud (2015); Antensteiner and Abidian (2017); Ouyang et al. (2017); Ganji et al. (2018); Pranti et al. (2018); Strauss et al. (2020)

[3] Wilks et al. (2009); Wilks (2011); Teixeira et al. (2022)

[4] Green et al. (2012); Baek et al. (2014b); Boehler et al. (2017); Gunapu et al. (2020)

[5] Castagnola, Maiolo, Maggiolini, Minotti, Marrani, Maita, Pecora, Angotzi, Ansaldo, Boffini, Fadiga, Fortunato and Ricci (2015)

[6] Castagnola et al. (2014); Lunghi et al. (2022)

[7] Castagnola, Descamps, Lecestre, Dahan, Remaud, Nowak and Bergaud (2015); Nikiforidis et al. (2020)

[8] Yamato et al. (1995); Bobacka (1999); Bobacka et al. (2000); Cui and Martin (2003); Xiao, Cui, Hancock, Bouguettaya, Reynolds and Martin (2004); Cui and Zhou (2007); Kayinamura et al. (2010); Luo et al. (2013); Baek et al. (2014a); Mandal et al. (2014); Kozai et al. (2015); Mandal et al. (2015); Gunapu and Vanjari (2017); Aqrawe et al. (2019); Decataldo et al. (2019); He et al. (2021); Lu et al. (2021); Xu et al. (2022)

[9] Gerwig et al. (2012); Samba et al. (2015)

[10] Teixeira et al. (2022)

[11] Antensteiner (2018)

[12] Teixeira et al. (2022)

- Perchlorate ion ($ClO_4$) -

[13] Yang and Martin (2006); King et al. (2011)

[14] Green et al. (2011, 2012); Baek et al. (2014b)

[15] Abidian et al. (2007); Yang et al. (2007); Abidian and Martin (2008); Abidian et al. (2009); Abidian and Martin (2009); Abidian et al. (2010); Kayinamura et al. (2010); Pigani et al. (2012); Baek et al. (2014a); Cysewska et al. (2015); Qu (2017); Chhin et al. (2018); Nikiforidis et al. (2020); Yang et al. (2021)

[16] Peng et al. (2007)

- p-Toluenesulfonate (pTS) -

[17] King et al. (2011)

[18] Green et al. (2009, 2010); Boretius et al. (2011); Green et al. (2011, 2012); Baek et al. (2014b); Green et al. (2013); Chapman et al. (2018)

[19] Kayinamura et al. (2010); Harris et al. (2012); Baek et al. (2014a)

- Multi-walled carbon nanotubes (MWCNT) -

[20] Kolarcik et al. (2014); Alba et al. (2015); Kozai et al. (2015)

[21] Luo et al. (2011); Zhou et al. (2013)

**Table 6.** Number of studies reporting each EDOT monomer concentration.

| Concentration (M) | 0.01[1] | 0.02[2] | 0.1[3] | 0.007[4] | 0.05[5] | 1[6] | 0.018[7] | N/A | Others* |
|---|---|---|---|---|---|---|---|---|---|
| Study count | 42 | 19 | 11 | 4 | 3 | 2 | 2 | 2 | 5 |

[1]Others included 0.0125 M (Kayinamura et al.; 2010), 0.015 M (Krukiewicz et al.; 2019), 0.2 M (Kozai et al.; 2015) 0.25 M (Peng et al.; 2007) and 0.5 M (Castagnola, Maiolo, Maggiolini, Minotti, Marrani, Maita, Pecora, Angotzi, Ansaldo, Boffini, Fadiga, Fortunato and Ricci; 2015).

[1] Yamato et al. (1995); Bobacka (1999); Bobacka et al. (2000); Cui and Martin (2003); Xiao, Cui and Martin (2004); Yang et al. (2005); Ludwig et al. (2006); Yang and Martin (2006); Abidian et al. (2007); Cui and Zhou (2007); Richardson-Burns et al. (2007); Yang et al. (2007); Abidian and Martin (2008); Abidian et al. (2009); Abidian and Martin (2009); Wilks et al. (2009); Abidian et al. (2010); King et al. (2011); Ludwig et al. (2011); Ouyang et al. (2011); Wilks (2011); Harris et al. (2012); Pigani et al. (2012); Zhou et al. (2013); Castagnola et al. (2014); Mandal et al. (2014); Cysewska et al. (2015); Kozai et al. (2015); Mandal et al. (2015); Charkhkar et al. (2016); Boehler et al. (2017); Ouyang et al. (2017); Qu (2017); Ganji et al. (2018); Pranti et al. (2018); Aqrawe et al. (2019); Bodart et al. (2019); Decataldo et al. (2019); Popov et al. (2019); Woeppel et al. (2019); Nikiforidis et al. (2020); Strauss et al. (2020); Lunghi et al. (2022)

[2] Xiao, Cui, Hancock, Bouguettaya, Reynolds and Martin (2004); Abidian et al. (2006); Luo et al. (2011); Gerwig et al. (2012); Luo et al. (2013); Kolarcik et al. (2014); Alba et al. (2015); Samba et al. (2015); Antensteiner and Abidian (2017); Gunapu and Vanjari (2017); Antensteiner (2018); Lee et al. (2017); Bodart et al. (2019); Gunapu et al. (2020); He et al. (2021); Lu et al. (2021); Xu et al. (2022)

[3] Cui and Martin (2003); Xiao, Cui, Hancock, Bouguettaya, Reynolds and Martin (2004); Bhandari et al. (2009); Green et al. (2009, 2010); Boretius et al. (2011); Green et al. (2011, 2012); Baek et al. (2014b); Green et al. (2013); Chapman et al. (2018)

[4] Nyberg et al. (2007); Venkatraman et al. (2011); Chen et al. (2013); Castagnola, Descamps, Lecestre, Dahan, Remaud, Nowak and Bergaud (2015)

[5] Baek et al. (2014a); Chhin et al. (2018); Yang et al. (2021)

[6] Sebaa et al. (2013); Zhang et al. (2018)

[7] Castagnola, Descamps, Lecestre, Dahan, Remaud, Nowak and Bergaud (2015); Teixeira et al. (2022)

**Table 7.** Number of studies reporting electrochemical impedance spectroscopy (EIS) excitation potential amplitudes.

| Amplitude (mV) | 5[1] | 10[2] | 20[3] | 25[4] | 30[5] | 40[6] | 50[7] | Other[*] |
|---|---|---|---|---|---|---|---|---|
| Study count | 21 | 14 | 6 | 2 | 2 | 3 | 2 | 4 |

* Others include 1.5 mV (Teixeira et al.; 2022), 24 mV (Qu; 2017), 100 mV (Pranti et al.; 2018), and 200 mV (Lee et al.; 2018).
17 studies did not report the EIS excitation amplitude.

[1] Cui and Martin (2003); Abidian et al. (2006); Cui and Zhou (2007); Yang et al. (2007); Abidian and Martin (2008); Abidian et al. (2009); Abidian and Martin (2009); Jan et al. (2009); Wilks et al. (2009); Abidian et al. (2010); King et al. (2011); Luo et al. (2011); Venkatraman et al. (2011); Wilks (2011); Castagnola et al. (2014); Kolarcik et al. (2014); Gunapu and Vanjari (2017); Popov et al. (2019); Gunapu et al. (2020); Strauss et al. (2020); Yang et al. (2021)

[2] Bobacka (1999); Bobacka et al. (2000); Boretius et al. (2011); Harris et al. (2012); Chen et al. (2013); Zhou et al. (2013); Castagnola, Maiolo, Maggiolini, Minotti, Marrani, Maita, Pecora, Angotzi, Ansaldo, Boffini, Fadiga, Fortunato and Ricci (2015); Alba et al. (2015); Boehler et al. (2017); Antensteiner (2018); Ganji et al. (2018); Aqrawe et al. (2018); Bodart et al. (2019); Nikiforidis et al. (2020)

[3] Luo et al. (2013); Mandal et al. (2014); Cysewska et al. (2015); Mandal et al. (2015); Charkhkar et al. (2016); He et al. (2021)

[4] Ludwig et al. (2006, 2011)

[5] Baek et al. (2014b,a)

[6] Green et al. (2009, 2010); Krukiewicz et al. (2019)

[7] Green et al. (2013); Castagnola, Descamps, Lecestre, Dahan, Remaud, Nowak and Bergaud (2015)

**Table 8.** Number of studies reporting electrochemical impedance spectroscopy (EIS) bias potentials.

| Potential vs OCP (V) | 0 V[1] | 0 V*[2] | 0.01 V*[3] | 0.2 V*[4] | 0.4 V*[4] | -0.2 V*[4] | -0.4 V*[4] |
|---|---|---|---|---|---|---|---|
| Study count | 18 | 5 | 2 | 1 | 1 | 1 | 1 |

* vs Ag|AgCl
45 studies did not report the EIS excitation amplitude.

[1] Cui and Martin (2003); Cui and Zhou (2007); Yang et al. (2007); Green et al. (2009, 2010); Luo et al. (2011); Gerwig et al. (2012); Luo et al. (2013); Zhou et al. (2013); Kolarcik et al. (2014); Mandal et al. (2014); Cysewska et al. (2015); Mandal et al. (2015); Boehler et al. (2017); Ganji et al. (2018); Krukiewicz et al. (2019); Gunapu et al. (2020); Yang et al. (2021)

[2] Bobacka et al. (2000); Peng et al. (2007); Harris et al. (2012); Bodart et al. (2019); Popov et al. (2019)

[3] Ouyang et al. (2017); Qu (2017)

[4] Bobacka et al. (2000)

**Table 9.** Number of studies reporting cyclic voltammetry (CV) sweep rates.

| **Sweep rate (mV/s)** | **10**[1] | **50**[2] | **100**[3] | **120**[4] | **150**[5] | **200**[6] | **500**[7] | **1000**[8] | **Others*** |
|---|---|---|---|---|---|---|---|---|---|
| **Study count** | 4 | 9 | 33 | 3 | 4 | 2 | 2 | 5 | 6 |

*Others included 5 mV/s (Bhandari et al.; 2009), 25 mV/s (Bobacka et al.; 2000), 30 mV/s (Popov et al.; 2019), 40 mV/s (Cysewska et al.; 2015), 70 mV/s (Popov et al.; 2019), 250 mV/s (Popov et al.; 2019).
2 studies did not report the CV sweep rate.

[1] Bobacka et al. (2000); Xiao, Cui and Martin (2004); Richardson-Burns et al. (2007); Frost et al. (2012)

[2] Bobacka et al. (2000); Wilks et al. (2009); Wilks (2011); Pigani et al. (2012); Zhou et al. (2013); Castagnola, Descamps, Lecestre, Dahan, Remaud, Nowak and Bergaud (2015); Lee et al. (2018); Popov et al. (2019); Lunghi et al. (2022)

[3] Yamato et al. (1995); Bobacka et al. (2000); Cui and Martin (2003); Xiao, Cui, Hancock, Bouguettaya, Reynolds and Martin (2004); Yang et al. (2005); Abidian et al. (2006); Yang and Martin (2006); Cui and Zhou (2007); Peng et al. (2007); Richardson-Burns et al. (2007); Abidian and Martin (2008, 2009); Jan et al. (2009); Abidian et al. (2010); King et al. (2011); Luo et al. (2011); Ouyang et al. (2011); Gerwig et al. (2012); Harris et al. (2012); Castagnola, Maiolo, Maggiolini, Minotti, Marrani, Maita, Pecora, Angotzi, Ansaldo, Boffini, Fadiga, Fortunato and Ricci (2015); Samba et al. (2015); Gunapu and Vanjari (2017); Ouyang et al. (2017); Antensteiner (2018); Chhin et al. (2018); Pranti et al. (2018); Aqrawe et al. (2018); Bodart et al. (2019); Popov et al. (2019); Woeppel et al. (2019); Gunapu et al. (2020); Nikiforidis et al. (2020); Yang et al. (2021)

[4] Green et al. (2009); Baek et al. (2014b,a)

[5] Green et al. (2011, 2012, 2013); Popov et al. (2019)

[6] Bobacka et al. (2000); Popov et al. (2019)

[7] Venkatraman et al. (2011); Chen et al. (2013)

[8] Wilks et al. (2009); Venkatraman et al. (2011); Alba et al. (2015); Strauss et al. (2020); Teixeira et al. (2022)

**Table 10.** Number of studies reporting current pulse (CP) polarity used for charge injection capacity (CIC) measurements.

| | **Cathodic First**[1] | **Anodic First**[2] |
|---|---|---|
| **Study count** | 15 | 5 |
| **Entry count** | 86 | 30 |

† To account for studies comparing several deposition methods we counted reported deposition method combinations (entries), for example a single study using two different co-ions would have study count 1, and entry count 2.

[1] Cui and Zhou (2007); Jan et al. (2009); Wilks et al. (2009); Luo et al. (2011); Venkatraman et al. (2011); Green et al. (2012, 2013); Zhou et al. (2013); Pranti et al. (2018); Aqrawe et al. (2018); Bodart et al. (2019); Woeppel et al. (2019); Gunapu et al. (2020); Nikiforidis et al. (2020); Strauss et al. (2020); Teixeira et al. (2022); Xu et al. (2022)

[2] Bobacka (1999); Green et al. (2011); Gerwig et al. (2012); Zhou et al. (2013); Mandal et al. (2015)

**Table 11.** Number of studies reporting current pulse (CP) pulse width used for charge injection capacity (CIC) measurements.

| **Pulse width ($\mu s$)** | **100**[1] | **200**[2] | **300**[1] | **400**[1] | **500**[3] | **600**[1] | **700**[1] | **800**[1] | **1000**[4] | **Others*** |
|---|---|---|---|---|---|---|---|---|---|---|
| **Study count** | 3 | 7 | 3 | 3 | 6 | 3 | 3 | 3 | 6 | 3 |

* Others include 90 $\mu s$ (Bodart et al.; 2019), 5 $ms$ (Gunapu et al.; 2020), 60 $s$ (Bobacka; 1999).

[1] Green et al. (2011, 2012, 2013)

[2] Wilks et al. (2009); Green et al. (2011, 2012, 2013); Zhou et al. (2013); Pranti et al. (2018); Nikiforidis et al. (2020)

[3] Jan et al. (2009); Green et al. (2011); Gerwig et al. (2012); Green et al. (2012, 2013); Strauss et al. (2020); Teixeira et al. (2022)

[4] Cui and Zhou (2007); Luo et al. (2011); Venkatraman et al. (2011); Mandal et al. (2015); Aqrawe et al. (2019); Woeppel et al. (2019); Xu et al. (2022)

**Table 12.** Number of studies reporting current pulse (CP) interpulse delay used for charge injection capacity (CIC) measurements.

| **Interpulse delay ($\mu$s)** | **200**[1] | **100**[2] | **50**[3] | **20**[4] | **10**[5] |
|---|---|---|---|---|---|
| **Study count** | 2 | 1 | 1 | 1 | 1 |

13 studies did not report an interpulse delay.

[1] Jan et al. (2009); Woeppel et al. (2019)
[2] Bodart et al. (2019)
[3] Pranti et al. (2018)
[4] Luo et al. (2011)
[5] Green et al. (2012)

## References

Abdullah, H. and Phairatana, T. (2022). A Study on the Performances of PEGDA and PEDOT: PSS Composite Resin for 3D-Printed Biosensor Applications, *ECS Transactions* **107**(1): 15001.

Abidian, M. R., Corey, J. M., Kipke, D. R. and Martin, D. C. (2010). Conducting-polymer nanotubes improve electrical properties, mechanical adhesion, neural attachment, and neurite outgrowth of neural electrodes, *Small* **6**(3): 421–429.

Abidian, M. R., Kim, D.-H. and Martin, D. C. (2006). Conducting-polymer nanotubes for controlled drug release, *Advanced materials* **18**(4): 405–409.

Abidian, M. R., Ludwig, K. A., Marzullo, T. C., Martin, D. C. and Kipke, D. R. (2009). Interfacing conducting polymer nanotubes with the central nervous system: chronic neural recording using poly (3, 4-ethylenedioxythiophene) nanotubes, *Advanced Materials* **21**(37): 3764–3770.

Abidian, M. R. and Martin, D. C. (2008). Experimental and theoretical characterization of implantable neural microelectrodes modified with conducting polymer nanotubes, *Biomaterials* **29**(9): 1273–1283.

Abidian, M. R. and Martin, D. C. (2009). Multifunctional nanobiomaterials for neural interfaces, *Advanced functional materials* **19**(4): 573–585.

Abidian, M. R., Salas, L. G., Yazdan-Shahmorad, A., Marzullo, T. C., Martin, D. C. and Kipke, D. R. (2007). In-vivo evaluation of chronically implanted neural microelectrode arrays modified with poly (3, 4-ethylenedioxythiophene) nanotubes, *2007 3rd International IEEE/EMBS Conference on Neural Engineering*, IEEE, pp. 61–64.

Adekoya, G. J., Sadiku, R. E. and Ray, S. S. (2021). Nanocomposites of pedot: Pss with graphene and its derivatives for flexible electronic applications: A review, *Macromolecular Materials and Engineering* **306**(3): 2000716.

Aggas, J. R., Abasi, S., Phipps, J. F., Podstawczyk, D. A. and Guiseppi-Elie, A. (2020). Microfabricated and 3-d printed electroconductive hydrogels of pedot:pss and their application in bioelectronics, *Biosensors and Bioelectronics* **168**: 112568.

Akbar, T. F., Tondera, C. and Minev, I. (2020). Conductive Hydrogels for Bioelectronic Interfaces, *in* L. Guo (ed.), *Neural Interface Engineering: Linking the Physical World and the Nervous System*, Springer International Publishing, pp. 237–265.

Alba, N. A., Du, Z. J., Catt, K. A., Kozai, T. D. and Cui, X. T. (2015). In vivo electrochemical analysis of a PEDOT/MWCNT neural electrode coating, *Biosensors* **5**(4): 618–646.

Antensteiner, M. (2018). *Fabrication and Investigation of Conducting Polymer Micro and Nano Structures for Bioelectronics Applications*, PhD thesis, University of Houston.

Antensteiner, M. and Abidian, M. R. (2017). Tunable nanostructured conducting polymers for neural interface applications, *2017 39th Annual International Conference of the IEEE Engineering in Medicine and Biology Society (EMBC)*, IEEE, pp. 1881–1884.

Aqrawe, Z., Montgomery, J., Travas-Sejdic, J. and Svirskis, D. (2018). Conducting polymers for neuronal microelectrode array recording and stimulation, *Sensors and Actuators B: Chemical* **257**: 753–765.

Aqrawe, Z., Wright, B., Patel, N., Vyas, Y., Malmstrom, J., Montgomery, J. M., Williams, D., Travas-Sejdic, J. and Svirskis, D. (2019). The influence of macropores on PEDOT/PSS microelectrode coatings for neuronal recording and stimulation, *Sensors and Actuators B: Chemical* **281**: 549–560.

Axpe, E., Orive, G., Franze, K. and Appel, E. A. (2020). Towards brain-tissue-like biomaterials, *Nature Communications* **11**(1).

Babaie, A., Bakhshandeh, B., Abedi, A., Mohammadnejad, J., Shabani, I., Ardeshirylajimi, A., Reza Moosavi, S., Amini, J. and Tayebi, L. (2020). Synergistic effects of conductive PVA/PEDOT electrospun scaffolds and electrical stimulation for more effective neural tissue engineering, *European Polymer Journal* **140**: 110051.

Baek, S., Green, R. A. and Poole-Warren, L. A. (2014a). The biological and electrical trade-offs related to the thickness of conducting polymers for neural applications, *Acta biomaterialia* **10**(7): 3048–3058.

Baek, S., Green, R. A. and Poole-Warren, L. A. (2014b). Effects of dopants on the biomechanical properties of conducting polymer films on platinum electrodes, *Journal of Biomedical Materials Research Part A* **102**(8): 2743–2754.

Bard, A. L. and Faulkner, L. R. (2001). *Electrochemical Methods Fundamentals and Applications*, 2nd edn, John Wiley & Sons.

Benoudjit, A., Bader, M. M. and Wan Salim, W. W. (2018). Study of electropolymerized PEDOT:PSS transducers for application as electrochemical sensors in aqueous media, *Sensing and Bio-Sensing Research* **17**: 18–24.

Bessaire, B., Mathieu, M., Salles, V., Yeghoyan, T., Celle, C., Simonato, J.-P. and Brioude, A. (2017). Synthesis of Continuous Conductive PEDOT:PSS Nanofibers by Electrospinning: A Conformal Coating for Optoelectronics, *ACS Applied Materials & Interfaces* **9**(1): 950–957.

Bhandari, S., Deepa, M., Srivastava, A. K., Joshi, A. G. and Kant, R. (2009). Poly (3, 4-ethylenedioxythiophene)- multiwalled carbon nanotube composite films: Structure-directed amplified electrochromic response and improved redox activity, *The Journal of Physical Chemistry B* **113**(28): 9416–9428.

Bhat, M. A., Rather, R. A. and Shalla, A. H. (2021). PEDOT and PEDOT:PSS conducting polymeric hydrogels: A report on their emerging applications, *Synthetic Metals* **273**: 116709.

Bianchi, M., De Salvo, A., Asplund, M., Carli, S., Di Lauro, M., Schulze-Bonhage, A., Stieglitz, T., Fadiga, L. and Biscarini, F. (2022). Poly(3,4-ethylenedioxythiophene)-Based Neural Interfaces for Recording and Stimulation: Fundamental Aspects and In Vivo Applications, *Advanced Science* **9**(12): 2104701.

Blinova, N. V., Stejskal, J., Trchová, M. and Prokeš, J. (2008). Control of polyaniline conductivity and contact angles by partial protonation, *Polymer International* **57**(1): 66–69.

Bobacka, J. (1999). Potential stability of all-solid-state ion-selective electrodes using conducting polymers as ion-to-electron transducers, *Analytical chemistry* **71**(21): 4932–4937.

Bobacka, J., Lewenstam, A. and Ivaska, A. (2000). Electrochemical impedance spectroscopy of oxidized poly (3, 4-ethylenedioxythiophene) film electrodes in aqueous solutions, *Journal of Electroanalytical Chemistry* **489**(1-2): 17–27.

Bodart, C., Rossetti, N., Hagler, J., Chevreau, P., Chhin, D., Soavi, F., Schougaard, S. B., Amzica, F. and Cicoira, F. (2019). Electropolymerized poly (3, 4-ethylenedioxythiophene)(PEDOT) coatings for implantable deep-brain-stimulating microelectrodes, *ACS applied materials & interfaces* **11**(19): 17226–17233.

Boehler, C., Carli, S., Fadiga, L., Stieglitz, T. and Asplund, M. (2020). Tutorial: guidelines for standardized performance tests for electrodes intended for neural interfaces and bioelectronics, *Nature Protocols* **15**(11): 3557–3578.

Boehler, C., Oberueber, F., Schlabach, S., Stieglitz, T. and Asplund, M. (2017). Long-term stable adhesion for conducting polymers in biomedical applications: Irox and nanostructured platinum solve the chronic challenge, *ACS applied materials & interfaces* **9**(1): 189–197.

Boretius, T., Schuettler, M. and Stieglitz, T. (2011). On the stability of poly-ethylenedioxythiopene as coating material for active neural implants, *Artificial organs* **35**(3): 245–248.

Brummer, S. and Turner, M. (1975). Electrical stimulation of the nervous system: the principle of safe charge injection with noble metal electrodes, *Bioelectrochemistry and Bioenergetics* **2**(1): 13–25.

Castagnola, E., Maiolo, L., Maggiolini, E., Minotti, A., Marrani, M., Maita, F., Pecora, A., Angotzi, G. N., Ansaldo, A., Boffini, M., Fadiga, L., Fortunato, G. and Ricci, D. (2015). PEDOT-CNT-Coated Low-Impedance, Ultra-Flexible, and Brain-Conformable Micro-ECoG Arrays, *IEEE Transactions on Neural Systems and Rehabilitation Engineering* **23**(3): 342–350.

Castagnola, V., Bayon, C., Descamps, E. and Bergaud, C. (2014). Morphology and conductivity of PEDOT layers produced by different electrochemical routes, *Synthetic metals* **189**: 7–16.

Castagnola, V., Descamps, E., Lecestre, A., Dahan, L., Remaud, J., Nowak, L. G. and

Bergaud, C. (2015). Parylene-based flexible neural probes with PEDOT coated surface for brain stimulation and recording, *Biosensors and Bioelectronics* **67**: 450–457.

Cea, C., Spyropoulos, G. D., Jastrzebska-Perfect, P., Ferrero, J. J., Gelinas, J. N. and Khodagholy, D. (2020). Enhancement-mode ion-based transistor as a comprehensive interface and real-time processing unit for in vivo electrophysiology, *Nature Materials* **19**(6): 679–686.

Chapman, C. A., Aristovich, K., Donega, M., Fjordbakk, C. T., Stathopoulou, T.-R., Viscasillas, J., Avery, J., Perkins, J. D. and Holder, D. (2018). Electrode fabrication and interface optimization for imaging of evoked peripheral nervous system activity with electrical impedance tomography (eit), *Journal of Neural Engineering* **16**(1): 016001.

Charkhkar, H., Knaack, G. L., McHail, D. G., Mandal, H. S., Peixoto, N., Rubinson, J. F., Dumas, T. C. and Pancrazio, J. J. (2016). Chronic intracortical neural recordings using microelectrode arrays coated with PEDOT–TFB, *Acta Biomaterialia* **32**: 57–67.

Chen, H.-l., Yang, D., Chen, C.-r., Tian, G.-z. and Kim, D.-H. (2022). In situ polymerization of conducting polymers around living neural cells: Cellular effect study, *Colloids and Surfaces B: Biointerfaces* **213**: 112410.

Chen, S., Pei, W., Gui, Q., Tang, R., Chen, Y., Zhao, S., Wang, H. and Chen, H. (2013). PEDOT/MWCNT composite film coated microelectrode arrays for neural interface improvement, *Sensors and Actuators A: Physical* **193**: 141–148.

Cheng, W., Liu, Y., Tong, Z., Zhu, Y., Cao, K., Chen, W., Zhao, D. and Yu, H. (2022). Micro-interfacial polymerization of porous PEDOT for printable electronic devices, *EcoMat* p. e12288.

Chhin, D., Polcari, D., Bodart-Le Guen, C., Tomasello, G., Cicoira, F. and Schougaard, S. B. (2018). Diazonium-based anchoring of PEDOT on Pt/Ir electrodes via diazonium chemistry, *Journal of The Electrochemical Society* **165**(12): G3066.

Chung, T., Wang, J. Q., Wang, J., Cao, B., Li, Y. and Pang, S. W. (2015). Electrode modifications to lower electrode impedance and improve neural signal recording sensitivity, *Journal of Neural Engineering* **12**(5): 056018.

Cogan, S. F. (2008). Neural stimulation and recording electrodes, *Annu. Rev. Biomed. Eng.* **10**: 275–309.

Cogan, S. F., Ludwig, K. A., Welle, C. G. and Takmakov, P. (2016). Tissue damage thresholds during therapeutic electrical stimulation, *Journal of neural engineering* **13**(2): 021001.

Cui, X., Hetke, J. F., Wiler, J. A., Anderson, D. J. and Martin, D. C. (2001). Electrochemical deposition and characterization of conducting polymer polypyrrole/PSS on multichannel neural probes, *Sensors and Actuators A: Physical* **93**(1): 8–18.

Cui, X. and Martin, D. C. (2003). Electrochemical deposition and characterization of poly (3, 4-ethylenedioxythiophene) on neural microelectrode arrays, *Sensors and Actuators B: Chemical* **89**(1-2): 92–102.

Cui, X. T. and Zhou, D. D. (2007). Poly (3, 4-ethylenedioxythiophene) for chronic neural stimulation, *IEEE Transactions on Neural Systems and Rehabilitation Engineering* **15**(4): 502–508.

Cysewska, K., Karczewski, J. and Jasiński, P. (2015). Influence of electropolymerization conditions on the morphological and electrical properties of PEDOT film, *Electrochimica Acta* **176**: 156–161.

Dauzon, E., Mansour, A. E., Niazi, M. R., Munir, R., Smilgies, D.-M., Sallenave, X., Plesse, C., Goubard, F. and Amassian, A. (2019). Conducting and Stretchable PEDOT:PSS Electrodes: Role of Additives on Self-Assembly, Morphology, and Transport, *ACS Applied Materials & Interfaces* **11**(19): 17570–17582.

Decataldo, F., Cramer, T., Martelli, D., Gualandi, I., Korim, W. S., Yao, S. T., Tessarolo, M., Murgia, M., Scavetta, E., Amici, R. et al. (2019). Stretchable low impedance electrodes for bioelectronic recording from small peripheral nerves, *Scientific reports* **9**(1): 1–9.

Depan, D. and Misra, R. (2014). The development, characterization, and cellular response of a novel electroactive nanostructured composite for electrical stimulation of neural cells, *Biomaterials science* **2**(12): 1727–1739.

Dijk, G., Kaszas, A., Pas, J. and O'Connor, R. P. (2022). Fabrication and in vivo 2-photon microscopy validation of transparent PEDOT:PSS microelectrode arrays, *Microsystems & Nanoengineering* **8**(1): 1–8.

Dominguez-Alfaro, A., Gabirondo, E., Alegret, N., De León-Almazán, C. M., Hernandez, R., Vallejo-Illarramendi, A., Prato, M. and Mecerreyes, D. (2021). 3D Printable Conducting and Biocompatible PEDOT-graft-PLA Copolymers by Direct Ink Writing, *Macromolecular Rapid Communications* **42**(12): 2100100.

Donahue, M. J., Kaszas, A., Turi, G. F., Rózsa, B., Slézia, A., Vanzetta, I., Katona, G., Bernard, C., Malliaras, G. G., Williamson, A. and et al. (2018). Multimodal characterization of neural networks using highly transparent electrode arrays, *eneuro* **5**(6).

Eickenscheidt, M., Singler, E. and Stieglitz, T. (2019). Pulsed electropolymerization of PEDOT enabling controlled branching, *Polymer Journal* **51**(10): 1029–1036.

Fan, B., Wolfrum, B. and Robinson, J. T. (2021). Impedance scaling for gold and platinum microelectrodes, *Journal of Neural Engineering* **18**(5): 056025.

Fan, L., Xiong, Y., Fu, Z., Xu, D., Wang, L., Chen, Y., Xia, H., Peng, N., Ye, S., Wang, Y., Zhang, L. and Ye, Q. (2017). Polyaniline promotes peripheral nerve regeneration by enhancement of the brain-derived neurotrophic factor and ciliary neurotrophic factor expression and activation of the ERK1/2/MAPK signaling pathway, *Molecular Medicine Reports* **16**(5): 7534–7540.

Frost, C. M., Wei, B., Baghmanli, Z., Cederna, P. S. and Urbanchek, M. G. (2012). PEDOT electrochemical polymerization improves electrode fidelity and sensitivity, *Plastic and reconstructive surgery* **129**(4): 933.

Fu, F., Wang, J. and Yu, J. (2021). Interpenetrating PAA-PEDOT conductive hydrogels for flexible skin sensors, *Journal of Materials Chemistry C* **9**(35): 11794–11800.

Furlani, F., Montanari, M., Sangiorgi, N., Saracino, E., Campodoni, E., Sanson, A., Benfenati, V., Tampieri, A., Panseri, S. and Sandri, M. (2022). Electroconductive and injectable hydrogels based on gelatin and PEDOT:PSS for a minimally invasive approach in nervous tissue regeneration, *Biomaterials Science* **10**(8): 2040–2053.

Ganji, M., Elthakeb, A. T., Tanaka, A., Gilja, V., Halgren, E. and Dayeh, S. A. (2017). Scaling effects on the electrochemical performance of poly(3,4-ethylenedioxythiophene (PEDOT), Au, and Pt for electrocorticography recording, *Advanced Functional Materials* **27**(42): 1703018.

Ganji, M., Hossain, L., Tanaka, A., Thunemann, M., Halgren, E., Gilja, V., Devor, A. and Dayeh, S. A. (2018). Monolithic and scalable au nanorod substrates improve PEDOT–metal adhesion and stability in neural electrodes, *Advanced healthcare materials* **7**(22): 1800923.

Garrudo, F. F. F., Chapman, C. A., Hoffman, P. R., Udangawa, R. W., Silva, J. C., Mikael, P. E., Rodrigues, C. A. V., Cabral, J. M. S., Morgado, J. M. F., Ferreira, F. C. and Linhardt, R. J. (2019). Polyaniline-polycaprolactone blended nanofibers for neural cell culture, *European Polymer Journal* **117**: 28–37.

Geddes, L. A. and Bourland, J. D. (1985). The strength-duration curve, *IEEE Transactions on Biomedical Engineering* **BME-32**(6): 458–459.

Gerwig, R., Fuchsberger, K., Schroeppel, B., Link, G. S., Heusel, G., Kraushaar, U., Schuhmann, W., Stett, A. and Stelzle, M. (2012). PEDOT–CNT composite microelectrodes for recording and electrostimulation applications: fabrication, morphology, and electrical properties, *Frontiers in neuroengineering* **5**: 8.

Ghasemi-Mobarakeh, L., Prabhakaran, M. P., Morshed, M., Nasr-Esfahani, M. H., Baharvand, H., Kiani, S., Al-Deyab, S. S. and Ramakrishna, S. (2011). Application of conductive polymers, scaffolds and electrical stimulation for nerve tissue engineering, *Journal of Tissue Engineering and Regenerative Medicine* **5**(4): e17–e35.

Gotovtsev, P. M., Badranova, G. U., Zubavichus, Y. V., Chumakov, N. K., Antipova, C. G., Kamyshinsky, R. A., Presniakov, M. Y., Tokaev, K. V. and Grigoriev, T. E. (2019). Electroconductive PEDOT:PSS-based hydrogel prepared by freezing-thawing method, *Heliyon* **5**(9): e02498.

Green, R. A., Hassarati, R. T., Bouchinet, L., Lee, C. S., Cheong, G. L., Jin, F. Y., Dodds, C. W., Suaning, G. J., Poole-Warren, L. A. and Lovell, N. H. (2012). Substrate dependent stability of conducting polymer coatings on medical electrodes, *Biomaterials* **33**(25): 5875–5886.

Green, R. A., Lovell, N. H. and Poole-Warren, L. A. (2009). Cell attachment functionality of bioactive conducting polymers for neural interfaces, *Biomaterials* **30**(22): 3637–3644.

Green, R. A., Lovell, N. H. and Poole-Warren, L. A. (2010). Impact of co-incorporating laminin peptide dopants and neurotrophic growth factors on conducting polymer properties, *Acta biomaterialia* **6**(1): 63–71.

Green, R., Duan, C., Hassarati, R., Goding, J., Byrnes-Preston, P., Suaning, G. J., Poole-Warren, L. and Lovell, N. H. (2011). Electrochemical stability of poly (ethylene dioxythiophene) electrodes, *2011 5th International IEEE/EMBS Conference on Neural Engineering*, IEEE, pp. 566–569.

Green, R., Matteucci, P., Hassarati, R., Giraud, B., Dodds, C., Chen, S., Byrnes-Preston, P., Suaning, G., Poole-Warren, L. and Lovell, N. (2013). Performance of conducting polymer electrodes for stimulating neuroprosthetics, *Journal of neural engineering* **10**(1): 016009.

Groenendaal, L., Jonas, F., Freitag, D., Pielartzik, H. and Reynolds, J. R. (2000). Poly(3,4-ethylenedioxythiophene) and Its Derivatives: Past, Present, and Future, *Advanced Materials* **12**(7): 481–494.

Gueye, M. N., Carella, A., Massonnet, N., Yvenou, E., Brenet, S., Faure-Vincent, J., Pouget, S., Rieutord, F., Okuno, H., Benayad, A., Demadrille, R. and Simonato, J.-P. (2016). Structure and dopant engineering in pedot thin films: Practical tools for a dramatic conductivity enhancement, *Chemistry of Materials* **28**(10): 3462–3468.

Guimard, N. K., Gomez, N. and Schmidt, C. E. (2007). Conducting polymers in biomedical engineering, *Progress in polymer science* **32**(8-9): 876–921.

Gunapu, D., Mudigunda, V. S., Das, A., Rengan, A. K. and Vanjari, S. R. K. (2020). Facile synthesis and characterization of poly (3, 4-ethylenedioxythiophene)/molybdenum disulfide (PEDOT/MoS2) composite coatings for potential neural electrode applications, *Journal of Applied Electrochemistry* **50**(9): 943–958.

Gunapu, D. S. K. and Vanjari, S. R. K. (2017). Preparation of high charge storage capacity PEDOT/functionalized mwcnts hybrid nanocomposite for neural electrode applications, *ECS Transactions* **77**(11): 1719.

Guo, L. (2020). Perspectives on electrical neural recording: a revisit to the fundamental concepts, *Journal of Neural Engineering* **17**(1): 013001.

Han, M. G. and Foulger, S. H. (2006). Facile Synthesis of Poly(3,4-ethylenedioxythiophene) Nanofibers from an Aqueous Surfactant Solution, *Small* **2**(10): 1164–1169.

Harris, A. R., Morgan, S. J., Chen, J., Kapsa, R. M., Wallace, G. G. and Paolini, A. G. (2012). Conducting polymer coated neural recording electrodes, *Journal of neural engineering* **10**(1): 016004.

Harris, A. R., Newbold, C., Carter, P., Cowan, R. and Wallace, G. G. (2018). Measuring the effective area and charge density of platinum electrodes for bionic devices, *Journal of Neural Engineering* **15**(4): 046015.

He, E., Xu, S., Xiao, G., Dai, Y., Li, X., Song, Y., Gao, F., Zhang, Y., Xu, S. and Cai, X. (2021). MWCNTs/PEDOT: PSS nanocomposites-modified microelectrode array for spatial dynamics recording of epileptic discharges in multi-subregion of hippocampal slice, *Sensors and Actuators B: Chemical* **329**: 129190.

Heo, D. N., Lee, S.-J., Timsina, R., Qiu, X., Castro, N. J. and Zhang, L. G. (2019). Development of 3d printable conductive hydrogel with crystallized pedot:pss for neural tissue engineering, *Materials Science and Engineering: C* **99**: 582–590.

Hosseini, E., Ozhukil Kollath, V. and Karan, K. (2020). The key mechanism of conductivity in PEDOT:PSS thin films exposed by anomalous conduction behaviour upon solvent-doping and sulfuric acid post-treatment, *Journal of Materials Chemistry C* **8**(12): 3982–3990.

Huang, W.-C., Lo, Y.-C., Chu, C.-Y., Lai, H.-Y., Chen, Y.-Y. and Chen, S.-Y. (2017). Conductive nanogel-interfaced neural microelectrode arrays with electrically controlled in-situ delivery of manganese ions enabling high-resolution MEMRI for synchronous neural tracing with deep brain stimulation, *Biomaterials* **122**: 141–153.

Hudak, E. M., Kumsa, D. W., Martin, H. B. and Mortimer, J. T. (2017). Electron transfer processes occurring on platinum neural stimulating electrodes: Calculated charge-storage capacities are inaccessible during applied stimulation, *Journal of Neural Engineering* **14**(4): 046012.

Ihalainen, P., Määttänen, A., Mattinen, U., Stępień, M., Bollström, R., Toivakka, M., Bobacka, J. and Peltonen, J. (2011). Electrodeposition of PEDOT-Cl film on a fully printed Ag/polyaniline electrode, *Thin Solid Films* **519**(7): 2172–2175.

Jan, E., Hendricks, J. L., Husaini, V., Richardson-Burns, S. M., Sereno, A., Martin, D. C. and Kotov, N. A. (2009). Layered carbon nanotube-polyelectrolyte electrodes outperform traditional neural interface materials, *Nano letters* **9**(12): 4012–4018.

Karimi-Soflou, R., Nejati, S. and Karkhaneh, A. (2021). Electroactive and antioxidant injectable in-situ forming hydrogels with tunable properties by polyethylenimine and polyaniline for nerve tissue engineering, *Colloids and Surfaces B: Biointerfaces* **199**: 111565.

Kayinamura, Y. P., Ovadia, M., Zavitz, D. and Rubinson, J. F. (2010). Investigation of near ohmic behavior for poly (3, 4-ethylenedioxythiophene): A model consistent with systematic variations in polymerization conditions, *ACS Applied Materials & Interfaces* **2**(9): 2653–2662.

Kim, D., Franco-Gonzalez, J. F. and Zozoulenko, I. (2021). How long are polymer chains in poly(3,4-ethylenedioxythiophene):tosylate films? an insight from molecular dynamics simulations, *The Journal of Physical Chemistry B* **125**(36): 10324–10334.

Kim, N., Kee, S., Lee, S. H., Lee, B. H., Kahng, Y. H., Jo, Y.-R., Kim, B.-J. and Lee, K. (2013). Highly conductive PEDOT:PSS nanofibrils induced by solution-processed crystallization, *Advanced Materials* **26**(14): 2268–2272.

King, Z. A., Shaw, C. M., Spanninga, S. A. and Martin, D. C. (2011). Structural, chemical and electrochemical characterization of poly (3, 4-ethylenedioxythiophene)(PEDOT) prepared with various counter-ions and heat treatments, *Polymer* **52**(5): 1302–1308.

Kitto, T., Bodart-Le Guen, C., Rossetti, N. and Cicoira, F. (2019). Processing and patterning of conducting polymers for flexible, stretchable, and biomedical electronics, *Handbook of Organic Materials for Electronic and Photonic Devices* p. 817–842.

Kolarcik, C. L., Catt, K., Rost, E., Albrecht, I. N., Bourbeau, D., Du, Z., Kozai, T. D., Luo, X., Weber, D. J. and Cui, X. T. (2014). Evaluation of poly (3, 4-ethylenedioxythiophene)/carbon nanotube neural electrode coatings for stimulation in the dorsal root ganglion, *Journal of neural engineering* **12**(1): 016008.

Kozai, T. D., Catt, K., Du, Z., Na, K., Srivannavit, O., Razi-ul, M. H., Seymour, J., Wise, K. D., Yoon, E. and Cui, X. T. (2015). Chronic in vivo evaluation of PEDOT/CNT for stable neural recordings, *IEEE Transactions on Biomedical Engineering* **63**(1): 111–119.

Krukiewicz, K., Chudy, M., Gregg, S. and Biggs, M. J. (2019). The synergistic effects of gold particles and dexamethasone on the electrochemical and biological performance of PEDOT neural interfaces, *Polymers* **11**(1): 67.

Lacour, S. P., Courtine, G. and Guck, J. (2016). Materials and technologies for soft implantable neuroprostheses, *Nature Reviews Materials* **1**(10).

Lee, D., Moon, H. C., Tran, B.-T., Kwon, D.-H., Kim, Y. H., Jung, S.-D., Joo, J. H. and Park, Y. S. (2018). Characterization of tetrodes coated with Au nanoparticles (AuNPs) and PEDOT and their application to thalamic neural signal detection in vivo, *Experimental neurobiology* **27**(6): 593.

Lee, W., Kim, D., Matsuhisa, N., Nagase, M., Sekino, M., Malliaras, G. G., Yokota, T. and Someya, T. (2017). Transparent, conformable, active multielectrode array using organic electrochemical transistors, *Proceedings of the National Academy of Sciences* **114**(40): 10554–10559.

Leleux, P., Badier, J.-M., Rivnay, J., Bénar, C., Hervé, T., Chauvel, P. and Malliaras, G. G. (2013). Conducting polymer electrodes for electroencephalography, *Advanced Healthcare Materials* **3**(4): 490–493.

Lerond, M., Cicoira, F. and G. Skene, W. (2022). Enhancing the performance of transparent and highly stretchable organic electrochemical transistors by acid treatment and copolymer blending of electrospun PEDOT:PSS fibers, *Journal of Materials Chemistry C* **10**(32): 11739–11746.

Li, H., Mao, P., Davis, M. and Yu, Z. (2021). PEDOT:PSS-polyethylene oxide

composites for stretchable and 3D-Printed thermoelectric devices, *Composites Communications* **23**: 100599.

Liu, J., Wei, B., Sloppy, J. D., Ouyang, L., Ni, C. and Martin, D. C. (2015). Direct imaging of the electrochemical deposition of poly(3,4-ethylenedioxythiophene) by transmission electron microscopy, *ACS Macro Letters* **4**(9): 897–900.

Liu, J., Zhuo, Y., Lu, J., Wang, L. and Ren, X. (2022). Novel Conductive rGO/PEDOT:PSS/PVA Nanofibers by Electrospinning, *Integrated Ferroelectrics* **229**(1): 305–312.

Liu, S., Zhao, Y., Hao, W., Zhang, X.-D. and Ming, D. (2020). Micro-and nanotechnology for neural electrode-tissue interfaces, *Biosensors and Bioelectronics* **170**: 112645.

Liu, Y.-C. and Hwang, B.-J. (2001). Mechanism of conductivity decay of polypyrrole exposed to water and enhancement of conductivity stability of copper(I)-modified polypyrrole, *Journal of Electroanalytical Chemistry* **501**(1): 100–106.

Lu, Y., Li, T., Zhao, X., Li, M., Cao, Y., Yang, H. and Duan, Y. Y. (2010). Electrodeposited polypyrrole/carbon nanotubes composite films electrodes for neural interfaces, *Biomaterials* **31**(19): 5169–5181.

Lu, Z., Xu, S., Wang, H., He, E., Liu, J., Dai, Y., Xie, J., Song, Y., Wang, Y., Wang, Y. et al. (2021). PtNPt/MWCNT-PEDOT: PSS-modified microelectrode arrays for the synchronous dopamine and neural spike detection in rat models of sleep deprivation, *ACS Applied Bio Materials* **4**(6): 4872–4884.

Ludwig, K. A., Langhals, N. B., Joseph, M. D., Richardson-Burns, S. M., Hendricks, J. L. and Kipke, D. R. (2011). Poly (3, 4-ethylenedioxythiophene)(PEDOT) polymer coatings facilitate smaller neural recording electrodes, *Journal of neural engineering* **8**(1): 014001.

Ludwig, K. A., Uram, J. D., Yang, J., Martin, D. C. and Kipke, D. R. (2006). Chronic neural recordings using silicon microelectrode arrays electrochemically deposited with a poly (3, 4-ethylenedioxythiophene)(PEDOT) film, *Journal of neural engineering* **3**(1): 59.

Lunghi, A., Mariano, A., Bianchi, M., Dinger, N. B., Murgia, M., Rondanina, E., Toma, A., Greco, P., Di Lauro, M., Santoro, F. et al. (2022). Flexible neural interfaces based on 3d PEDOT:PSS micropillar arrays, *Advanced Materials Interfaces* **9**(25): 2200709.

Luo, X., Weaver, C. L., Tan, S. and Cui, X. T. (2013). Pure graphene oxide doped conducting polymer nanocomposite for bio-interfacing, *Journal of Materials Chemistry B* **1**(9): 1340–1348.

Luo, X., Weaver, C. L., Zhou, D. D., Greenberg, R. and Cui, X. T. (2011). Highly stable carbon nanotube doped poly (3, 4-ethylenedioxythiophene) for chronic neural stimulation, *Biomaterials* **32**(24): 5551–5557.

Mandal, H. S., Kastee, J. S., McHail, D. G., Rubinson, J. F., Pancrazio, J. J. and Dumas, T. C. (2015). Improved poly (3, 4-ethylenedioxythiophene)(PEDOT) for

neural stimulation, *Neuromodulation: Technology at the Neural Interface* **18**(8): 657–663.

Mandal, H. S., Knaack, G. L., Charkhkar, H., McHail, D. G., Kastee, J. S., Dumas, T. C., Peixoto, N., Rubinson, J. F. and Pancrazio, J. J. (2014). Improving the performance of poly (3, 4-ethylenedioxythiophene) for brain–machine interface applications, *Acta biomaterialia* **10**(6): 2446–2454.

Merrill, D. R., Bikson, M. and Jefferys, J. G. (2005). Electrical stimulation of excitable tissue: design of efficacious and safe protocols, *Journal of neuroscience methods* **141**(2): 171–198.

Mierzejewski, M., Steins, H., Kshirsagar, P. and Jones, P. D. (2020). The noise and impedance of microelectrodes, *Journal of Neural Engineering* **17**(5): 052001.

Morris, J. D., Thourson, S. B., Panta, K. R., Flanders, B. N. and Payne, C. K. (2017). Conducting polymer nanowires for control of local protein concentration in solution, *Journal of Physics D: Applied Physics* **50**(17): 174003.

Murbach, J. M., Currlin, S., Widener, A., Tong, Y., Chhatre, S., Subramanian, V., Martin, D. C., Johnson, B. N. and Otto, K. J. (2018). In situ electrochemical polymerization of poly (3, 4-ethylenedioxythiophene)(PEDOT) for peripheral nerve interfaces, *MRS communications* **8**(3): 1043–1049.

Nardes, A. M. (2007). On the conductivity of PEDOT: PSS thin films, *Tech. Univ. Eindh* **132**.

Newman, J. (1966). Resistance for Flow of Current to a Disk, *Journal of The Electrochemical Society* **113**(5): 501.

Ngoensawat, U., Pisuchpen, T., Sritana-anant, Y., Rodthongkum, N. and Hoven, V. P. (2022). Conductive electrospun composite fibers based on solid-state polymerized Poly(3,4-ethylenedioxythiophene) for simultaneous electrochemical detection of metal ions, *Talanta* **241**: 123253.

Nguyen, J. K., Park, D. J., Skousen, J. L., Hess-Dunning, A. E., Tyler, D. J., Rowan, S. J., Weder, C. and Capadona, J. R. (2014). Mechanically-compliant intracortical implants reduce the neuroinflammatory response, *Journal of Neural Engineering* **11**(5): 056014.

Nie, S., Li, Z., Yao, Y. and Jin, Y. (2021). Progress in Synthesis of Conductive Polymer Poly(3,4-Ethylenedioxythiophene), *Frontiers in Chemistry* **9**.

Nikiforidis, G., Wustoni, S., Routier, C., Hama, A., Koklu, A., Saleh, A., Steiner, N., Druet, V., Fiumelli, H. and Inal, S. (2020). Benchmarking the performance of electropolymerized poly (3, 4-ethylenedioxythiophene) electrodes for neural interfacing, *Macromolecular Bioscience* **20**(11): 2000215.

Niu, H., Liu, Y., Song, H., Meng, Q., Du, Y. and Shen, S. Z. (2021). Facile preparation of flexible all organic PEDOT:PSS/methyl cellulose thermoelectric composite film by a screen printing process, *Synthetic Metals* **276**: 116752.

Nyberg, T., Shimada, A. and Torimitsu, K. (2007). Ion conducting polymer microelectrodes for interfacing with neural networks, *Journal of Neuroscience Methods* **160**(1): 16–25.

Ouyang, J. (2013). "secondary doping" methods to significantly enhance the conductivity of pedot:pss for its application as transparent electrode of optoelectronic devices, *Displays* **34**(5): 423–436.

Ouyang, L. (2014). *Crosslinking, electrografting and in vivo polymerization of Poly(3,4-ethylenedioxythiophene) (PEDOT) and derivatives as reliable neural interfacing materials*, Ph.D., University of Delaware, United States – Delaware. ISBN: 9781321607352.

Ouyang, L., Green, R., Feldman, K. E. and Martin, D. C. (2011). Direct local polymerization of poly (3, 4-ethylenedioxythiophene) in rat cortex, *Progress in brain research*, Vol. 194, Elsevier, pp. 263–271.

Ouyang, L., Wei, B., Kuo, C.-c., Pathak, S., Farrell, B. and Martin, D. C. (2017). Enhanced PEDOT adhesion on solid substrates with electrografted p (edot-nh2), *Science advances* **3**(3): e1600448.

Peng, C., Jin, J. and Chen, G. Z. (2007). A comparative study on electrochemical co-deposition and capacitance of composite films of conducting polymers and carbon nanotubes, *Electrochimica Acta* **53**(2): 525–537.

Petrova, G. I. (1999). Influence of electrode impedance changes on the common-mode rejection ratio in bioimpedance measurements, *Physiological Measurement* **20**(4): N11.

Pigani, L., Heras, A., Colina, , Seeber, R. and López-Palacios, J. (2004). Electropolymerisation of 3,4-ethylenedioxythiophene in aqueous solutions, *Electrochemistry Communications* **6**(11): 1192–1198.

Pigani, L., Zanfrognini, B. and Seeber, R. (2012). PEDOT-modified microelectrodes. preparation, characterisation and analytical performances, *Electroanalysis* **24**(6): 1340–1347.

Pingree, L. S., MacLeod, B. A. and Ginger, D. S. (2008). The changing face of PEDOT:PSS films: substrate, bias, and processing effects on vertical charge transport, *The Journal of Physical Chemistry C* **112**(21): 7922–7927.

Popov, A., Brasiunas, B., Mikoliunaite, L., Bagdziunas, G., Ramanavicius, A. and Ramanaviciene, A. (2019). Comparative study of polyaniline (PANI), poly (3, 4-ethylenedioxythiophene)(PEDOT) and PANI-PEDOT films electrochemically deposited on transparent indium thin oxide based electrodes, *Polymer* **172**: 133–141.

Poverenov, E., Li, M., Bitler, A. and Bendikov, M. (2010). Major effect of electropolymerization solvent on morphology and electrochromic properties of PEDOT films, *Chemistry of Materials* **22**(13): 4019–4025.

Pranti, A. S., Schander, A., Bödecker, A. and Lang, W. (2018). PEDOT:PSS coating on gold microelectrodes with excellent stability and high charge injection capacity for chronic neural interfaces, *Sensors and Actuators B: Chemical* **275**: 382–393.

Proctor, C. M., Rivnay, J. and Malliaras, G. G. (2016). Understanding volumetric capacitance in conducting polymers, *Journal of Polymer Science Part B: Polymer Physics* **54**(15): 1433–1436.

Proctor, C. M., Slézia, A., Kaszas, A., Ghestem, A., del Agua, I., Pappa, A.-M., Bernard, C., Williamson, A. and Malliaras, G. G. (2018). Electrophoretic drug delivery for seizure control, *Science Advances* **4**(8).

Qu, J. (2017). *Electrochemically deposited conducting polymers for reliable biomedical interfacing materials: formulation, mechanical characterization, and failure analysis*, PhD thesis, University of Delaware.

Rastin, H., Zhang, B., Bi, J., Hassan, K., Tung, T. T. and Losic, D. (2020). 3d printing of cell-laden electroconductive bioinks for tissue engineering applications, *Journal of Materials Chemistry B* **8**(27): 5862–5876.

Ren, X., Yang, M., Yang, T., Xu, C., Ye, Y., Wu, X., Zheng, X., Wang, B., Wan, Y. and Luo, Z. (2021). Highly Conductive PPy–PEDOT:PSS Hybrid Hydrogel with Superior Biocompatibility for Bioelectronics Application, *ACS Applied Materials & Interfaces* **13**(21): 25374–25382.

Richardson-Burns, S. M., Hendricks, J. L., Foster, B., Povlich, L. K., Kim, D.-H. and Martin, D. C. (2007). Polymerization of the conducting polymer poly (3, 4-ethylenedioxythiophene)(PEDOT) around living neural cells, *Biomaterials* **28**(8): 1539–1552.

Ritzau-Reid, K. I., Spicer, C. D., Gelmi, A., Grigsby, C. L., Ponder Jr., J. F., Bemmer, V., Creamer, A., Vilar, R., Serio, A. and Stevens, M. M. (2020). An Electroactive Oligo-EDOT Platform for Neural Tissue Engineering, *Advanced Functional Materials* **30**(42): 2003710.

Rivnay, J., Inal, S., Collins, B. A., Sessolo, M., Stavrinidou, E., Strakosas, X., Tassone, C., Delongchamp, D. M. and Malliaras, G. G. (2016). Structural control of mixed ionic and electronic transport in conducting polymers, *Nature communications* **7**(1): 1–9.

Rossetti, N., Hagler, J., Kateb, P. and Cicoira, F. (2021). Neural and electromyography pedot electrodes for invasive stimulation and recording, *Journal of Materials Chemistry C* **9**(23): 7243–7263.

Samba, R., Herrmann, T. and Zeck, G. (2015). PEDOT-CNT coated electrodes stimulate retinal neurons at low voltage amplitudes and low charge densities, *Journal of neural engineering* **12**(1): 016014.

Sanchez-Sanchez, A., del Agua, I., Malliaras, G. G. and Mecerreyes, D. (2019). Conductive Poly(3,4-Ethylenedioxythiophene) (PEDOT)-Based Polymers and Their Applications in Bioelectronics, *in* M. R. Aguilar and J. San Román (eds), *Smart Polymers and their Applications (Second Edition)*, Woodhead Publishing in Materials, Woodhead Publishing, pp. 191–218.

Sebaa, M. A., Dhillon, S. and Liu, H. (2013). Electrochemical deposition and evaluation of electrically conductive polymer coating on biodegradable magnesium implants for

neural applications, *Journal of Materials Science: Materials in Medicine* **24**(2): 307–316.

Sezen-Edmonds, M. and Loo, Y.-L. (2017). Beyond doping and charge balancing: How polymer acid templates impact the properties of conducting polymer complexes, *The Journal of Physical Chemistry Letters* **8**(18): 4530–4539.

Shahrim, N. A., Ahmad, Z., Wong Azman, A., Fachmi Buys, Y. and Sarifuddin, N. (2021). Mechanisms for doped pedot:pss electrical conductivity improvement, *Materials Advances* **2**(22): 7118–7138.

Shi, H., Liu, C., Jiang, Q. and Xu, J. (2015). Effective Approaches to Improve the Electrical Conductivity of PEDOT:PSS: A Review, *Advanced Electronic Materials* **1**(4): 1500017.

Simon, D. T., Gabrielsson, E. O., Tybrandt, K. and Berggren, M. (2016). Organic bioelectronics: bridging the signaling gap between biology and technology, *Chemical reviews* **116**(21): 13009–13041.

Sinha, S. K., Noh, Y., Reljin, N., Treich, G. M., Hajeb-Mohammadalipour, S., Guo, Y., Chon, K. H. and Sotzing, G. A. (2017). Screen-printed pedot:pss electrodes on commercial finished textiles for electrocardiography, *ACS Applied Materials & Interfaces* **9**(43): 37524–37528.

Sordini, L., Garrudo, F. F., Rodrigues, C. A., Linhardt, R. J., Cabral, J. M., Ferreira, F. C. and Morgado, J. (2021). Effect of electrical stimulation conditions on neural stem cells differentiation on cross-linked pedot:pss films, *Frontiers in Bioengineering and Biotechnology* **9**.

Stejskal, J. and Gilbert, R. G. (2002). Polyaniline. Preparation of a conducting polymer(IUPAC Technical Report), *Pure and Applied Chemistry* **74**(5): 857–867.

Stiller, A., Black, B., Kung, C., Ashok, A., Cogan, S., Varner, V. and Pancrazio, J. (2018). A meta-analysis of intracortical device stiffness and its correlation with histological outcomes, *Micromachines* **9**(9): 443.

Stiller, A. M., Basavarajappa, L., Brown, K., Voit, W., Pancrazio, J. J. and Hoyt, K. (2019). Elastrographic assessment of micromotion-induced strain in tissue adjacent to intracortical implants in rat, *2019 IEEE International Ultrasonics Symposium (IUS)* .

Strauss, I., Niederhoffer, T., Giannotti, A., Panarese, A. M., Bernini, F., Gabisonia, K., Ottaviani, M. M., Petrini, F. M., Recchia, F. A., Raspopovic, S. et al. (2020). Q-pine: A quick to implant peripheral intraneural electrode, *Journal of Neural Engineering* **17**(6): 066008.

Subramanian, V. and Martin, D. C. (2021). Direct observation of liquid-to-solid phase transformations during the electrochemical deposition of poly(3,4-ethylenedioxythiophene) (PEDOT) by liquid-phase transmission electron microscopy (LPTEM), *Macromolecules* **54**(14): 6956–6967.

Tamburri, E., Orlanducci, S., Toschi, F., Terranova, M. L. and Passeri, D. (2009). Growth mechanisms, morphology, and electroactivity of PEDOT layers produced by electrochemical routes in aqueous medium, *Synthetic metals* **159**(5-6): 406–414.

Teixeira, H., Dias, C., Veloso, R., Apolinário, A. and Ventura, J. (2022). Tuning PEDOT:PSS low-impedance thin films with high charge injection for microelectrodes applications, *Progress in Organic Coatings* **168**: 106894.

Thourson, S. B. and Payne, C. K. (2017). Modulation of action potentials using PEDOT:PSS conducting polymer microwires, *Scientific reports* **7**(1): 1–7.

Tomaskovic-Crook, E., Zhang, P., Ahtiainen, A., Kaisvuo, H., Lee, C.-Y., Beirne, S., Aqrawe, Z., Svirskis, D., Hyttinen, J., Wallace, G. G., Travas-Sejdic, J. and Crook, J. M. (2019). Human Neural Tissues from Neural Stem Cells Using Conductive Biogel and Printed Polymer Microelectrode Arrays for 3D Electrical Stimulation, *Advanced Healthcare Materials* **8**(15): 1900425.

Tseghai, G. B., Malengier, B., Fante, K. A., Nigusse, A. B. and Van Langenhove, L. (2020). Development of a flex and stretchy conductive cotton fabric via flat screen printing of pedot:pss/pdms conductive polymer composite, *Sensors* **20**(6): 1742.

Vėbraitė, I. and Hanein, Y. (2021). Soft devices for high-resolution neuro-stimulation: The interplay between low-rigidity and resolution, *Frontiers in Medical Technology* **3**.

Venkatraman, S., Hendricks, J., King, Z. A., Sereno, A. J., Richardson-Burns, S., Martin, D. and Carmena, J. M. (2011). In vitro and in vivo evaluation of PEDOT microelectrodes for neural stimulation and recording, *IEEE Transactions on Neural Systems and Rehabilitation Engineering* **19**(3): 307–316.

Vernitskaya, T. V. and Efimov, O. N. (1997). Polypyrrole: a conducting polymer; its synthesis, properties and applications, *Russian Chemical Reviews* **66**(5): 443. Publisher: IOP Publishing.

Wang, A., Jung, D., Lee, D. and Wang, H. (2021). Impedance characterization and modeling of subcellular to micro-sized electrodes with varying materials and PEDOT:PSS coating for bioelectrical interfaces, *ACS Applied Electronic Materials* **3**(12): 5226–5239.

Wang, K., Tian, L., Wang, T., Zhang, Z., Gao, X., Wu, L., Fu, B. and Liu, X. (2019). Electrodeposition of alginate with PEDOT/PSS coated MWCNTs to make an interpenetrating conducting hydrogel for neural interface, *Composite Interfaces* **26**(1): 27–40.

Wang, P., Wang, M., Zhu, J., Wang, Y., Gao, J., Gao, C. and Gao, Q. (2021). Surface engineering via self-assembly on PEDOT: PSS fibers: Biomimetic fluff-like morphology and sensing application, *Chemical Engineering Journal* **425**: 131551.

Wang, Y., Zhu, C., Pfattner, R., Yan, H., Jin, L., Chen, S., Molina-Lopez, F., Lissel, F., Liu, J., Rabiah, N. I. and et al. (2017). A highly stretchable, transparent, and conductive polymer, *Science Advances* **3**(3).

Wellman, S. M., Eles, J. R., Ludwig, K. A., Seymour, J. P., Michelson, N. J., McFadden, W. E., Vazquez, A. L. and Kozai, T. D. Y. (2018). A Materials Roadmap to Functional Neural Interface Design, *Advanced Functional Materials* **28**(12): 1701269.

Wilks, S. J. (2011). *Enhancing the intracortical neural interface with poly (3, 4-ethylenedioxythiophene)(PEDOT)*, PhD thesis, Purdue University.

Wilks, S. J., Richardson-Burn, S. M., Hendricks, J. L., Martin, D. and Otto, K. J. (2009). Poly (3, 4-ethylene dioxythiophene)(PEDOT) as a micro-neural interface material for electrostimulation, *Frontiers in neuroengineering* **2**: 7.

Woeppel, K. M., Zheng, X. S., Schulte, Z. M., Rosi, N. L. and Cui, X. T. (2019). Nanoparticle doped PEDOT for enhanced electrode coatings and drug delivery, *Advanced healthcare materials* **8**(21): 1900622.

Worfolk, B. J., Andrews, S. C., Park, S., Reinspach, J., Liu, N., Toney, M. F., Mannsfeld, S. C. B. and Bao, Z. (2015). Ultrahigh electrical conductivity in solution-sheared polymeric transparent films, *Proceedings of the National Academy of Sciences* **112**(46): 14138–14143.

Xiao, Y., Cui, X., Hancock, J. M., Bouguettaya, M., Reynolds, J. R. and Martin, D. C. (2004). Electrochemical polymerization of poly (hydroxymethylated-3, 4-ethylenedioxythiophene)(PEDOT-MeOH) on multichannel neural probes, *Sensors and Actuators B: Chemical* **99**(2-3): 437–443.

Xiao, Y., Cui, X. and Martin, D. C. (2004). Electrochemical polymerization and properties of PEDOT/S-EDOT on neural microelectrode arrays, *Journal of Electroanalytical Chemistry* **573**(1): 43–48.

Xu, S., Deng, Y., Luo, J., He, E., Liu, Y., Zhang, K., Yang, Y., Xu, S., Sha, L., Song, Y. et al. (2022). High-throughput PEDOT: PSS/PtNPs-modified microelectrode array for simultaneous recording and stimulation of hippocampal neuronal networks in gradual learning process, *ACS Applied Materials & Interfaces* **14**(13): 15736–15746.

Xue, J., Wu, T., Dai, Y. and Xia, Y. (2019). Electrospinning and electrospun nanofibers: Methods, materials, and applications, *Chemical Reviews* **119**(8): 5298–5415.

Yamato, H., Ohwa, M. and Wernet, W. (1995). Stability of polypyrrole and poly (3, 4-ethylenedioxythiophene) for biosensor application, *Journal of Electroanalytical Chemistry* **397**(1-2): 163–170.

Yang, J., Kim, D. H., Hendricks, J. L., Leach, M., Northey, R. and Martin, D. C. (2005). Ordered surfactant-templated poly (3, 4-ethylenedioxythiophene)(PEDOT) conducting polymer on microfabricated neural probes, *Acta Biomaterialia* **1**(1): 125–136.

Yang, J., Lipkin, K. and Martin, D. C. (2007). Electrochemical fabrication of conducting polymer poly (3, 4-ethylenedioxythiophene)(PEDOT) nanofibrils on microfabricated neural prosthetic devices, *Journal of Biomaterials Science, Polymer Edition* **18**(8): 1075–1089.

Yang, J. and Martin, D. C. (2006). Impedance spectroscopy and nanoindentation of conducting poly (3, 4-ethylenedioxythiophene) coatings on microfabricated neural prosthetic devices, *Journal of Materials Research* **21**(5): 1124–1132.

Yang, M., Yang, T., Deng, H., Wang, J., Ning, S., Li, X., Ren, X., Su, Y., Zang, J., Li, X. et al. (2021). Poly (5-nitroindole) thin film as conductive and adhesive interfacial layer for robust neural interface, *Advanced Functional Materials* **31**(49): 2105857.

Yuk, H., Lu, B., Lin, S., Qu, K., Xu, J., Luo, J. and Zhao, X. (2020). 3d printing of conducting polymers, *Nature Communications* **11**(1).

Zhang, C., Driver, N., Tian, Q., Jiang, W. and Liu, H. (2018). Electrochemical deposition of conductive polymers onto magnesium microwires for neural electrode applications, *Journal of Biomedical Materials Research Part A* **106**(7): 1887–1895.

Zhang, S., Kumar, P., Nouas, A. S., Fontaine, L., Tang, H. and Cicoira, F. (2015). Solvent-induced changes in pedot:pss films for organic electrochemical transistors, *APL Materials* **3**(1): 014911.

Zhang, Y.-F., Guo, M.-M., Zhang, Y., Tang, C. Y., Jiang, C., Dong, Y., Law, W.-C. and Du, F.-P. (2020). Flexible, stretchable and conductive PVA/PEDOT:PSS composite hydrogels prepared by SIPN strategy, *Polymer Testing* **81**: 106213.

Zhou, H., Cheng, X., Rao, L., Li, T. and Duan, Y. Y. (2013). Poly (3, 4-ethylenedioxythiophene)/multiwall carbon nanotube composite coatings for improving the stability of microelectrodes in neural prostheses applications, *Acta biomaterialia* **9**(5): 6439–6449.

Zubair, N. A., Rahman, N. A., Lim, H. N., Zawawi, R. M. and Sulaiman, Y. (2016). Electrochemical properties of PVA–GO/PEDOT nanofibers prepared using electrospinning and electropolymerization techniques, *RSC Advances* **6**(21): 17720–17727. Publisher: The Royal Society of Chemistry.